The Role of Steady Phosphodiesterase Activity in the Kinetics and Sensitivity of the Light-adapted Salamander Rod Photoresponse

S. Nikonov,* T.D. Lamb,‡ and E.N. Pugh Jr.*

From the *Department of Ophthalmology and Institute of Neurological Sciences, University of Pennsylvania, Philadelphia, Pennsylvania 19104; and ‡Department of Physiology, University of Cambridge, Cambridge, CB2 3EG, United Kingdom

ABSTRACT We investigated the kinetics and sensitivity of photocurrent responses of salamander rods, both in darkness and during adaptation to steady backgrounds producing 20–3,000 photoisomerizations per second, using suction pipet recordings. The most intense backgrounds suppressed 80% of the circulating dark current and decreased the flash sensitivity ~30-fold. To investigate the underlying transduction mechanism, we expressed the responses as a fraction of the steady level of cGMP-activated current recorded in the background. The fractional responses to flashes of any fixed intensity began rising along a common trajectory, regardless of background intensity. We interpret these invariant initial trajectories to indicate that, at these background intensities, light adaptation does not alter the gain of any of the amplifying steps of phototransduction. For subsaturating flashes of fixed intensity, the fractional responses obtained on backgrounds of different intensity were found to "peel off" from their common initial trajectory in a background-dependent manner: the more intense the background, the earlier the time of peeling off. This behavior is consistent with a background-induced reduction in the effective lifetime of at least one of the three major integrating steps in phototransduction; i.e., an acceleration of one or more of the following: (1) the inactivation of activated rhodopsin (R*); (2) the inactivation of activated phosphodiesterase (E*, representing the complex G_α–PDE of phosphodiesterase with the transducin α-subunit); or (3) the hydrolysis of cGMP, with rate constant β. Our measurements show that, over the range of background intensities we used, β increased on average to ~20 times its dark-adapted value; and our theoretical analysis indicates that this increase in β is the primary mechanism underlying the measured shortening of time-to-peak of the dim-flash response and the decrease in sensitivity of the fractional response.

KEY WORDS: photoreceptors • G-protein cascade • sensory transduction • light adaptation • cGMP hydrolysis

INTRODUCTION

In the presence of background illumination, rod photoreceptors adjust their sensitivity and response kinetics over an intensity range of several decades, and cone photoreceptors do so over an even greater range of intensities. Over the years, a number of investigators have studied the dependence of the rod's steady photocurrent and flash sensitivity on the intensity of background illumination. Other investigators have measured a shortening of the effective lifetime of cGMP (using an "IBMX-jump" protocol), and a shortening of the apparent lifetime of activated rhodopsin (monitored with bright flashes) during steady illumination. In other studies, it has been reported that the amplification of phototransduction is reduced during light adaptation.

In the present work the aim of our experiments has been to investigate all of these properties in the same population of rod photoreceptors. Thus, in an ideal experiment we have attempted: (1) to measure the steady state response versus intensity relation; (2) to measure families of flash responses on a range of backgrounds, from very dim flashes (to determine flash sensitivity) up to very bright flashes (to determine the dominant time constant of recovery); (3) to measure responses to steps of isobutyl methylxanthine (IBMX),[1] both in darkness and on backgrounds (to determine the steady-state rate constant of cGMP hydrolysis); and (4) to measure "step/flash" behavior, which permits estimation of the lifetime of activated rhodopsin. In practice, it has not been feasible to perform all these experiments on an individual rod, but, in a population of about a dozen rods recorded for up to 4 h, we were able to perform several of the procedures on each.

In a recent quantitative study of light adaptation using truncated salamander rods, Koutalos et al. (1995a,b) investigated the contributions of guanylyl cyclase activity and phosphodiesterase activity to the overall light adaptation behavior of the cells. One of our goals has been to extend their analysis of the steady state by focusing on the role of the phosphodiesterase activity, which we have measured using the "IBMX-jump" method. Another goal has been to characterize

Address correspondence to E.N. Pugh Jr., University of Pennsylvania, Department of Ophthalmology, Stellar-Chance Building, 422 Curie Boulevard, Philadelphia, PA 19104-6069. Fax: (215) 573-7155; E-mail: pugh@mail.med.upenn.edu

[1]*Abbreviations used in this paper:* IBMX, isobutyl methylxanthine; PDE, phosphodiesterase.

the effects of adaptation-dependent changes in the principal integrating steps of phototransduction, which include the following: the lifetime of R*; the lifetime of the active phosphodiesterase complex (PDE*); and the lifetime of cGMP, which is the reciprocal of the instantaneous rate constant of cGMP hydrolysis. As an aid to achieving these goals, we developed a molecular model of the complete set of reactions mediating transduction and adaptation, and solved the equations to obtain the steady state response versus intensity relation. In addition, we have integrated the equations numerically, so as to predict the kinetic responses and to examine the dependence of the solutions on the time constants of the principal integrating steps.

Our main conclusions are, first, that the gain of the activation steps in transduction is unaltered during light adaptation; and, second, that much of the acceleration in kinetics and desensitization of the biochemical cascade arises from the increased rate constant of cGMP hydrolysis resulting from light-stimulated PDE activity. The negative feedback loop mediated by Ca^{2+} concentration acts to prevent the suppression of circulating current that would otherwise occur and, in this way, the drop in Ca^{2+} concentration rescues the cell from the saturation that would occur in the absence of adaptational mechanisms. A preliminary and qualitative description of some of these results has been presented by Pugh et al. (1999).

MATERIALS AND METHODS

Suction Pipet Recordings

Our methods for preparing isolated salamander rods and for recording and analyzing their electrical responses have been reported previously (Lyubarsky et al., 1996; Nikonov et al., 1998). The photocurrents were low pass–filtered at 150 Hz (4-pole Butterworth) and sampled at 300 Hz; the delay introduced by this filtering was measured as 5.5 ms at the 50% response to a step input, and as 5.4 ms for a ramp input. All records were analyzed at full bandwidth, and are presented in the figures at full bandwidth, unless otherwise specified.

For all the experiments reported here, the rod's inner segment was drawn into a suction pipet, which recorded the circulating current, while the protruding outer segment was continually superfused with a standard amphibian Ringer's solution (Lyubarsky et al., 1996). In "IBMX-jump" experiments, the outer segment was briefly exposed to a test solution containing 500 μM IBMX (a competitive inhibitor of phosphodiesterase), by rapid translation of a laminar-flow boundary across the cell. This procedure was used to estimate the activity of guanylyl cyclase (and, thereby, the phosphodiesterase activity in the steady state before the jump) in the manner developed by Hodgkin and Nunn (1988).

To obtain enough information to make the required quantitative calculations for an individual rod, we found it necessary to hold the cell for at least an hour, and in the best experiments, we achieved stable recordings for >4 h. A summary of the stability of our recordings is presented in Fig. 1, which plots the amplitudes of saturating responses obtained under dark-adapted conditions over the entire recording duration, for each of the nine rods that provided the core observations presented in this paper. (Data from five additional rods recorded for ~1 h are also included in some summary figures.)

Light Stimuli

Light stimuli were monochromatic (500 nm, bandwidth 8 nm), circularly polarized, and generated via one of two optical channels: (1) a tungsten halogen lamp illuminating a grating monochromator, followed by a shutter; and (2) a xenon flash lamp (flash duration, 20 μs) filtered by an interference filter. In all experiments using backgrounds, the steady illumination was provided by the shuttered incandescent beam, and the flashes came from the xenon flash lamp. For some experiments in dark-

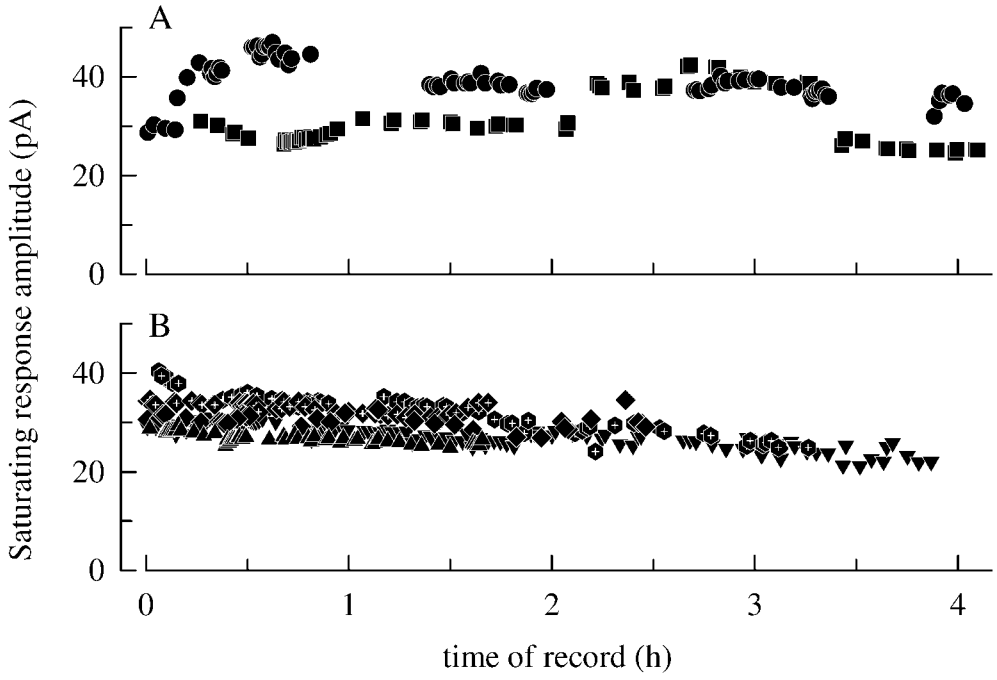

FIGURE 1. History of the responses of the principal rods of the experiments. Each point represents the response to a saturating flash presented to a rod after two or more minutes of dark adaptation. (A) Histories of rods *a* and *c* of Table II presented separately from those of the other rods (B) for clarity. The gaps in the response histories represent periods when the rods were exposed to background lights or to IBMX. (B) Histories of the seven additional principal rods.

adapted conditions, the flashes were delivered using the shuttered beam, and the flash duration was 22 ms. Flash intensities (Φ) are given in estimated numbers of photoisomerizations per outer segment, calculated by multiplying the measured flux density of the flash at the image plane (in photons per square micrometer) by the estimated outer segment collecting area of 18 μm^2 for salamander rods (Baylor et al., 1979; Lyubarsky et al., 1996). Steady intensities (I) are similarly given in photoisomerizations per second. For results taken from other investigations, we have adopted a collecting area of 20 μm^2 for circularly polarized (or unpolarized) light, and 40 μm^2 for linearly polarized light, as was generally used in those studies.

Light Adaptation Protocol

Dark-adapted rods were exposed to steps of light of calibrated intensity for periods of ~2 min. Beginning at least 20 s after the onset of the background, a number of test flashes were delivered at separations sufficient to allow full recovery. These were followed by a saturating flash, to determine the circulating current remaining in the presence of the background, and after recovery from this bright flash, the background was extinguished. The cycle was repeated for a series of test flash intensities, and the entire procedure was repeated for a range of background intensities. Control experiments established that the time course of the response to the saturating flash was unchanged over the epoch of the background from 20 s to 2 min. In some experiments (the step/flash protocol), a saturating flash was delivered at the instant the background was extinguished, as in Fain et al. (1989).

Numerical Integration of Equations

A complete set of equations describing transduction in the G-protein cascade is set out in the APPENDICES. To solve these equations numerically, we coded the equations independently in our two laboratories, using Matlab (The Mathworks), and the programs are available at http://www.physiol.cam.ac.uk/staff/Lamb/RodSim and upon request. The solutions to both steady state and time-varying equations obtained with the two programs agreed very closely.

Simulated Responses to Steps of IBMX

To simulate responses to steps of IBMX in darkness or during steady backgrounds (for the analysis in Fig. 7), we adopted the following procedures. The value of β was reduced according to the competitive inhibition factor given in Eq. A15, which specifies a time constant (τ_I) for equilibration of the concentration of IBMX in the outer segment with that in the perfusate. Previous experiments had shown that the time for completion of the movement of the laminar boundary across the rod is ~100 ms (Lyubarsky et al., 1996). Therefore, we initially set τ_I to this value, and varied it to obtain the best fit to the earliest onset of increased current over the family of background intensities; we found that the best fit was obtained with τ_I = 100 ms, and so we maintained this value throughout.

To begin with, the values of all parameters were set to those of the standard rod (see APPENDIX A). The value of β_{Dark} for the particular rod was determined as that which provided the best fitting simulation to the IBMX step in darkness; this value invariably agreed to within 10% of that obtained using the Hodgkin and Nunn (1988) method of analysis (which is described in RESULTS). The amplification constant (A) of the rod was extracted by analysis of the rising phase of the flash response family obtained in the dark-adapted state; this analysis differed from that of Lamb and Pugh (1992), in that the activation model incorporating the membrane time constant (Smith and Lamb, 1997) was used. Finally, for each IBMX step in light-adapted conditions, the value of I was found that minimized the sum-of-squares error between experiment and prediction over the first 200 ms of the response. From this value of I, the value of $\beta(I)$ was found by substitution in Eq. B7. From the steepness of the variation in the sum-of-squares error with variation in β (see Fig. 8 E), we think that our extracted estimates of β are reliable to within about ±10%.

THEORY

In this section, we examine ways of quantifying the PDE activity that underlies the rod's electrical response. We show that a fundamentally important parameter that must be extracted is the fractional opening of cGMP-activated channels, which we denote as F. To estimate this parameter, we need to express the rod's response (and/or circulating current) in fractional terms. Similarly, we have found it important to express the rod's sensitivity in terms of the fractional response; as we shall show, we thereby avoid the effects of "response compression" and obtain a measure of the intrinsic biochemical adaptation.

Symbols and Terminology

The three independent variables of our analysis are t, Φ, and I, where t is the time after a stimulus delivering Φ photoisomerizations to the rod, in the presence of a steady background intensity of I photoisomerizations per second. Four important dependent variables that we will use in this section are as follows: $f(t)$, the proportion of cGMP-activated channels open; $j(t)$, the circulating current; $r(t)$, the response expressed as the change in this current; and s, the sensitivity. Note that we use lowercase symbols to denote the absolute values of these dependent variables. We will now distinguish two ways of normalizing these variables, and in an effort to avoid ambiguity, we will adopt two different terms to refer to these different types of normalization, which are summarized in Table I.

First, we will use the term "fractional" to indicate that the circulating current has been divided by its steady state value, and that the response and sensitivity have been calculated from this fractional current. We will denote these fractional parameters using the corresponding uppercase symbols $J(t)$, $R(t)$, and S. Furthermore, we will denote steady state values obtained on a background of intensity (I) by writing them in the form $j(I)$, $\beta(I)$, etc. Thus, the fractional circulating current is defined as $J(t) = j(t)/j(I)$, and the fractional response as $R(t) = r(t)/j(I)$, where $r(t) = j(I) - j(t)$. Hence, $R(t)$ is the complement of $J(t)$; i.e., $R(t) = 1 - J(t)$. The absolute sensitivity is defined as $s = r(t_{peak})/\Phi$, in the limit of dim flashes (where, by convention, r is measured at the peak); hence, the fractional sensitivity is defined as $S = R(t_{peak})/\Phi$.

To distinguish our second way of normalizing, we will use the term "relative" to indicate that a steady value is

TABLE I

Absolute, Fractional, and Relative Values of Variables

	Symbol	Description	Definition
Absolute values	$f(t)$	Proportion of channels open, as a function of time	
	$f(I)$	Proportion of channels open, in the steady state	
	$j(t)$	Circulating current, as a function of time(pA)	
	$j(I)$	Circulating current, in the steady state (pA)	
	$r(t)$	Response, as a function of time (pA)	$r(t) = j(I) - j(t)$
	$s(I)$	Absolute sensitivity (pA/isomerization)	$s = r(t_{peak}) / \Phi$
Fractional values	$F(t)$	Channel opening	$F(t) = f(t)/f(I)$
	$J(t)$	Fractional circulating current	$J(t) = j(t)/j(I)$
	$R(t)$	Fractional response	$R(t) = r(t)/r(I)$
	$S(I)$	Fractional sensitivity	$S = R(t_{peak})/\Phi$
Relative values	$F_{rel}(I)$	Relative channel opening	$F_{rel}(I) = f(I)/f_{Dark}$
	$J_{rel}(I)$	Relative circulating current	$J_{rel}(I) = j(I)/j_{Dark}$
	$s_{rel}(I)$	Relative sensitivity	$s_{rel}(I) = s(I)/s_{Dark}$
	$S_{rel}(I)$	Relative fractional sensitivity	$S_{rel}(I) = S(I)/S_{Dark}$

The term "absolute" refers to raw measurements. The term "fractional" is used here to refer to normalization of a variable with respect to the steady level (of channel opening or current) in the adapted state. The term "relative" is used here to denote normalization of a steady value with respect to the corresponding value in dark-adapted conditions. See THEORY.

expressed relative to its value in darkness. Thus, the relative circulating current is $J_{rel}(I) = j(I)/j_{Dark}$, whereas the relative sensitivity is $s_{rel} = s/s_{Dark}$, and the relative fractional sensitivity is $S_{rel} = S/S_{Dark}$.

Fractional cGMP-activated Current and Response

The importance of expressing the circulating current (and/or the response) in fractional terms is that this immediately provides us with an estimate of the fractional level of channel opening, which in turn gives us the cGMP concentration, and (as we will show) thereby provides information about the underlying PDE activity.

The cGMP-activated opening of channels is described by the Hill relation, Eq. A6, as

$$f = \frac{cG^{n_{cG}}}{cG^{n_{cG}} + K_{cG}^{n_{cG}}} \approx \left(\frac{cG}{K_{cG}}\right)^{n_{cG}}, \quad (1)$$

where $f(t)$ is the absolute proportion of cGMP-activated channels open, $cG(t)$ is the free concentration of cGMP, n_{cG} is the Hill coefficient, and $K_{cG}(t)$ is the half-activation concentration. The approximation on the right applies because the cGMP concentration is always much smaller than the half-activation concentration. Hence, the fractional opening of cGMP-gated channels (i.e., expressed as a fraction of the steady-state level) is defined as

$$F(t) = \frac{f(t)}{f(I)} \approx \left(\frac{cG(t)}{cG(I)} \Big/ \frac{K_{cG}(t)}{K_{cG}(I)}\right)^{n_{cG}}. \quad (2)$$

We have adopted the symbol F for this variable for consistency with our previous notation (Lamb and Pugh, 1992).

At sufficiently early times in the response to any stimulus, the Ca^{2+} concentration $Ca(t)$ will have changed negligibly from the steady-state level $Ca(I)$, and, therefore, it will be acceptable to regard $K_{cG}(t)$ in Eq. 2 as unchanged from the steady value $K_{cG}(I)$, even though $K_{cG}(t)$ will change at later times through modulation of the channels by Ca^{2+}-calmodulin (see Eq. A11). Accordingly, at early times in any response, the fractional opening of channels $F(t)$ will approximate to

$$F(t) \approx \left(\frac{cG(t)}{cG(I)}\right)^{n_{cG}}. \quad (3)$$

Now, provided that the cGMP-activated current j_{cG} is directly proportional to the number of channels open (i.e., independent of membrane voltage) then $J_{cG}(t) = F(t)$, and we can write

$$F(t) \approx \left(\frac{cG(t)}{cG(I)}\right)^{n_{cG}} \approx J_{cG}(t) = 1 - R_{cG}(t), \quad (4)$$

where the subscript "$_{cG}$" has been introduced to denote the cGMP-activated component of J or R.

Eq. 4 shows that, even in the presence of steady background illumination, and in the face of changes in the steady magnitude of $K_{cG}(I)$ in different adaptational states, the fractional cGMP concentration at early times can be extracted simply by measuring the fractional cGMP-activated current; i.e., we can use $R_{cG}(t)$ to provide a measure of $cG(t)/cG(I)$.

In practice, a complication arises in calculating the cGMP-activated component of current j_{cG} because we can only measure the total outer segment current j_{tot}, which is the sum of j_{cG} and the electrogenic exchange current j_{ex}. Unfortunately, we do not have a direct measure of the time course of the latter (small) component, except for the special case of a strongly saturating flash. However numerical simulations (not presented) indicate that over the early rising phase of the flash response, it is adequate to ignore the time dependence of $j_{ex}(t)$, and simply approximate it as constant; i.e., $j_{ex}(t) \approx j_{ex}(I)$. Thus, at early times, we can approximate the fractional response $R_{cG}(t)$ required in Eq. 4 as

$$R_{cG}(t) \approx \frac{r_{tot}(t)}{j_{cG}(I)} = \frac{j_{tot}(I) - j_{tot}(t)}{j_{tot}(I) - j_{ex}(I)}. \quad (5)$$

A graphical illustration of this normalization is shown in Fig. 2 B, where a scale for R_{cG} is plotted at the right, running from zero at the steady-state level of measured

current to a value of unity at the level of current reached shortly after an extremely bright flash (i.e., at the initial level of the exchange current). One needs to be aware that the approximation in Eq. 5 breaks down at later times, when $j_{ex}(t)$ changes. In view of this limitation, we will use Eq. 5 to evaluate the response $R(t)$ in Eq. 4 only when we are examining the early phase of light responses. In other cases, on a slower time base, when $j_{ex}(t)$ is expected to change substantially, we will simply determine $R(t)$ with respect to the total current by calculating $R_{tot}(t) = r_{tot}(t)/j_{tot}(I)$.

Relation between PDE Activity and Circulating Current

By considering the differential equation for the synthesis and hydrolysis of cGMP, Lamb and Pugh (1992) derived an expression for the flash-induced increase, $\Delta\beta(t)$, in the rate constant of cGMP hydrolysis, from its dark-adapted level β_{Dark}, in terms of the current scaled to the dark level. Since we have now shown that a comparable scaling is applicable for steady backgrounds, rather than just in darkness, Lamb and Pugh's Equation 6.18 can be extended to the general form

$$\Delta\beta(t) = \beta(t) - \beta(I) = -\frac{1}{n_{cG}}\left[\frac{d}{dt}\ln F(t)\right] + \beta(I)\left(F(t)^{-\frac{1}{n_{cG}}} - 1\right). \quad (6)$$

At sufficiently early times, when $F(t) \approx 1$, the final term in this expression approaches zero, so that $\Delta\beta(t)$ is given by the first term, in which the only variable is the fractional opening of cGMP-activated channels, $F(t)$, which we have shown is given by $1 - R_{cG}(t)$ (Eq. 4).

The important conclusion from this equation is that, if, at sufficiently early times, it can be shown experimentally that the fractional response $R_{cG}(t)$ has a common initial phase in the presence of different backgrounds then the initial time course of PDE activation underlying the responses must also be the same on the different backgrounds.

Relative Steady-state Current

Since $F(t)$ expresses the channel activation as a fraction of its steady-state level, it must always start from unity. But another parameter of considerable interest is the steady-state level of channel activation in a steady background, relative to its dark-adapted level, which we denote as $F_{rel}(I) = f(I)/f_{Dark}$. If we again assume that the circulating current $j(I)$ is directly proportional to channel opening $f(I)$, then we have

$$F_{rel}(I) \approx J_{rel}(I) = \frac{j(I)}{j_{Dark}}. \quad (7)$$

Koutalos et al. (1995b) have shown that, in the steady state, the exchange current $j_{ex}(I)$ is directly proportional to the cGMP-activated current $j_{cG}(I)$ (see Eq. A4), so that the relative steady-state current $F_{rel}(I)$ will be the same whether Eq. 7 is evaluated using j_{cG} or using j_{tot}.

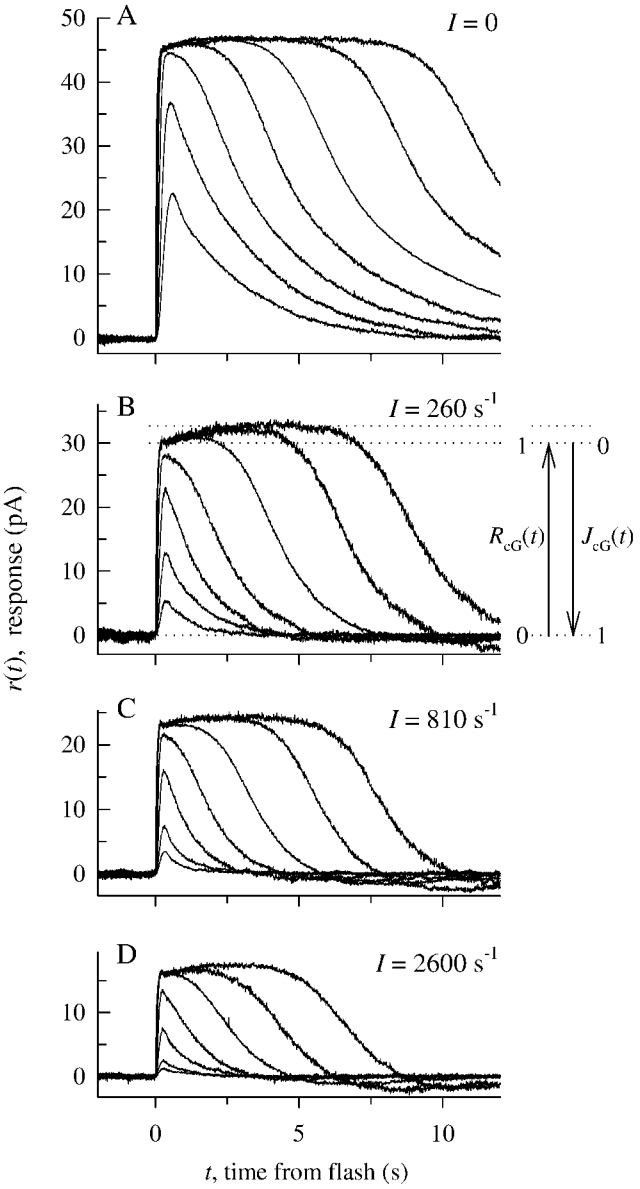

FIGURE 2. Photocurrent response families of a salamander rod, obtained under four conditions of adaptation: in darkness (A) and in the presence of steady background lights of the indicated intensities (I) in photoisomerizations per second (B–D). Each of the four families presents averaged responses $r(t)$ to the same sequence of flashes, estimated to produce Φ = 260, 830, 2,600, 8,300, 26,000, 83,000, and 260,000 photoisomerizations per flash. Each trace is averaged from at least 5 responses, but up to 30 responses were averaged to produce the responses with smallest amplitudes. Rod *a* of Table II. The additional scales at the right of B provide graphical definitions of the fractional cGMP-activated current $J_{cG}(t)$ and response $R_{cG}(t)$, according to Eqs. 4 and 5.

Fractional Sensitivity of the Flash Response

According to our analysis above, the transduction process may be probed at the level of PDE activity by first converting the absolute response (r) to fractional response (R), and in the same way the rod's sensitivity may

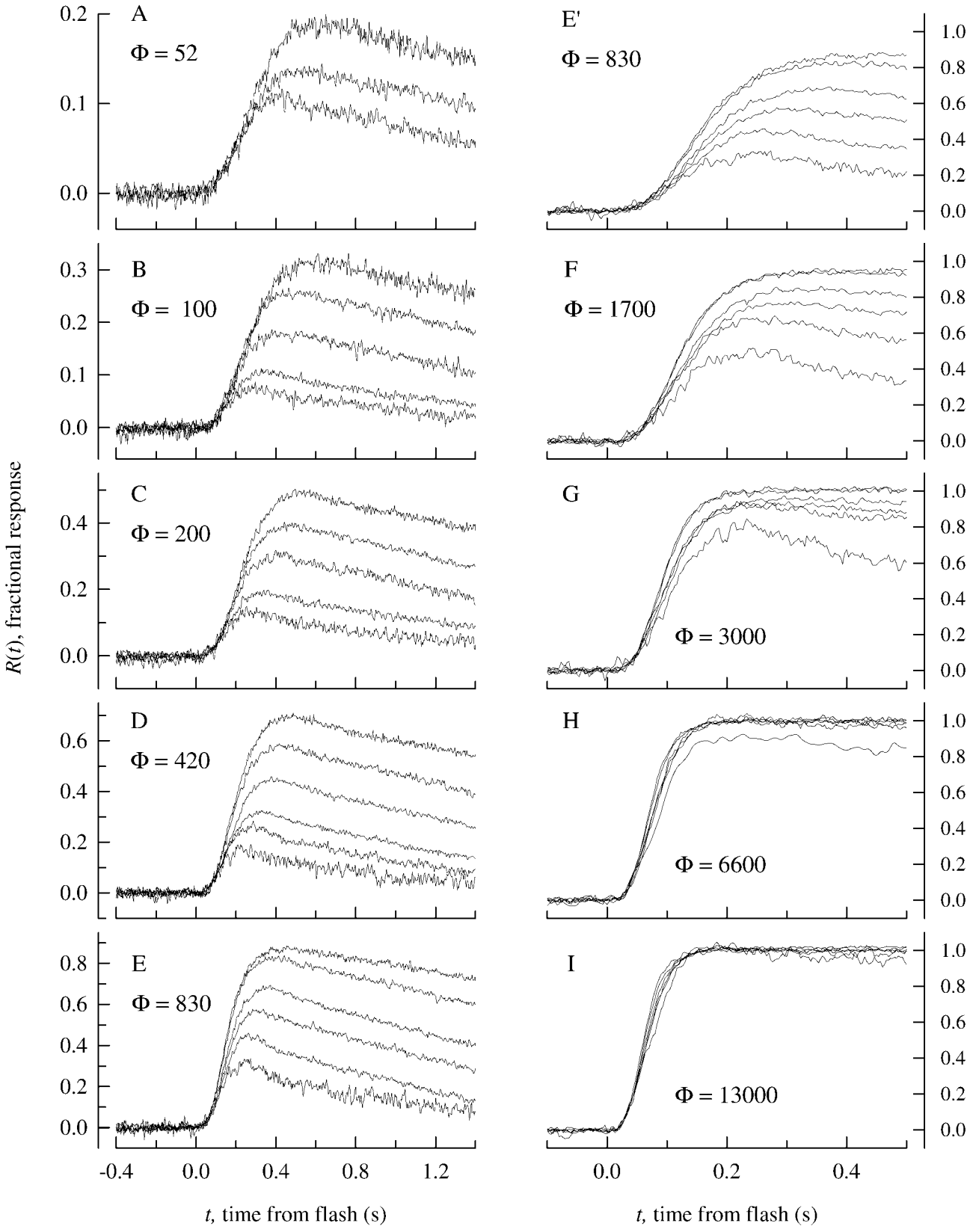

FIGURE 3. Fractional responses of a rod under six conditions of adaptation: dark adapted, and in the presence of steady backgrounds producing I = 19, 60, 190, 600, and 1,900 photoisomerizations per second. The responses are expressed as a fraction of the maximal cGMP-activated current in each adaptational condition; i.e., as $R_{cG}(t) \approx r_{tot}(t) / j_{cG}(I)$, estimated according to Eq. 5 and the scale in Fig. 2 B. Each panel illustrates responses to flashes of a single intensity, at the indicated value of Φ, in photoisomerizations; responses to the more intense flashes (right column) are presented on a shorter time scale, and the responses to Φ = 830 photoisomerizations are repeated on both scales (E and E′). Each trace shown is the average from at least 5 trials, with up to 30 trials being averaged for the smallest amplitude traces. Rod *b* of Table II.

TABLE II

Parameters of Individual Rods

Rod	Figures	Symbols	Recorded j_{cG}	A	β_{Dark}	τ_E	$\frac{\alpha_{min}}{\alpha_{max}}$
			pA	s^{-2}	s^{-1}	*s*	
a	1, 2, 5, 6, 8, 9, 11, 12	●	38	0.042	1.0	1.6	0.013
b	1, 3–6, 9–11	■	32	0.092	1.6	1.5	0.05
c	1, 6, 9–11	◆	30	0.083	1.3	1.7	0.015
d	1, 7, 8, 6–11	⊕	31	0.100	1.3	1.5	0.02
e	1, 6, 9–11	▲	27	0.125	1.5	1.8	0.06
f	1, 6, 9–11	▼	27	0.046	0.9	2.7	0.02
g	1, 6, 9–11	⊕	33	0.083	1.5	1.7	0.05
h	1, 6, 9, 11	▼	25	0.067	0.8	2.7	0.02
i	1, 6, 9, 11	▲	44	0.029	0.9	1.9	0.05
j	6	▲	25	0.100		2.3	0.04
k	6	▼	21	0.133		2.6	0.03
Mean ± SD			30.3 ± 6.5	0.082 ± 0.033	1.2 ± 0.3	2.0 ± 0.5	0.033 ± 0.016

Column 1 identifies individual rods. Column 2 indicates figures in the paper in which data of the rod appears. Column 3 provides the symbol used throughout the paper for data of the rod. Column 4 (j_{cG}) is the mean amplitude (measured at 250–300 ms) of responses to strongly saturating flashes delivered over the entire experiment (see Figs. 1, and 3 I). Column 5 gives the amplification constant (A) estimated by fitting the activation model of Lamb and Pugh (1992), modified to incorporate the membrane time constant (Smith and Lamb, 1997). Column 6 gives the estimate of rate constant of cGMP hydrolysis in the dark (β_{Dark}) as measured with the methods illustrated in Figs. 7 and 8. Column 7 gives the time constant of inactivation of the PDE, estimated by the "Pepperberg plot" method illustrated in Fig. 5 (see also Fig. 11). Column 8 gives the ratio of calcium-insensitive cyclase activity to maximum cyclase activity (Eq. A10), estimated from fitting of the model to the IBMX jump data in darkness (Fig. 8); calcium sensitivity is manifest as a deceleration of the rate of increase in current after the jump.

be corrected for "response compression" by measuring the fractional sensitivity, $S = R/\Phi$. The sensitivity parameter that is conventionally plotted is the relative sensitivity $s_{rel} = s/s_{Dark}$ (in the past, this has often been denoted as S_F/S_F^D, but we avoid that terminology here since F denotes fractional opening of channels). This measure of raw sensitivity may be converted to the fractional form $S_{rel} = S/S_{Dark}$ simply by dividing it by the relative circulating current $J_{rel}(I)$, because of the following relations:

$$S_{rel}(I) = \frac{S(I)}{S_{Dark}} = \frac{s(I)/j(I)}{s_{Dark}/j_{Dark}} = \frac{s_{rel}(I)}{J_{rel}(I)}. \quad (8)$$

The crucial insight is that use of the relative fractional sensitivity (S_{rel}) in Eq. 8 removes the response compression that results from a reduced steady-state level of circulating current. The application of this concept will be illustrated in Fig. 5.

RESULTS

Flash Response Families in Dark-adapted and Light-adapted Conditions

Fig. 2 presents families of flash responses from one rod under four adaptation conditions: darkness, and in the presence of steady illumination estimated to produce I = 260, 810, and 2,600 photoisomerizations per second. An identical series of seven flashes was delivered in each panel, and the traces of raw response $r(t)$ clearly show the hallmarks of light adaptation: progressive reduction in sensitivity; a decrease in time to peak of the dim-flash response; and earlier recovery from a bright flash, in the presence of successively brighter backgrounds. For example, under the four conditions of adaptation, the dimmest flash suppressed 20, 4.7, 3, and 1.1 pA of circulating current, and the peak response occurred at 0.6, 0.38, 0.34, and 0.30 s, respectively. For the most intense flash, the time taken to reach 50% recovery was 12.3, 9.1, 7.8, and 6.6 s in the four conditions.

There are conflicting reports in the literature as to whether part of photoreceptor desensitization during light adaptation is brought about by a reduction in the gain of any of the "amplification" steps underlying activation of the G-protein cascade. This has been investigated through examination of the early rising phase of light-adapted responses. On the one hand, Torre et al. (1986) and Fain et al. (1989) have reported that this early rising phase is unaltered by adaptation to weak backgrounds, even though the recovery phase occurs earlier. On the other hand, both Gray-Keller and Detwiler (1994) and Jones (1995) have reported that the early rising phase of the response is attenuated, and that their results indicate a reduction in the amplification constant of transduction. Likewise, Lagnado and Baylor (1994) have reported that, in the presence of lowered intracellular Ca^{2+} concentration, the gain of activation is reduced. In view of these differences, one of the principal aims of our experiments has been to

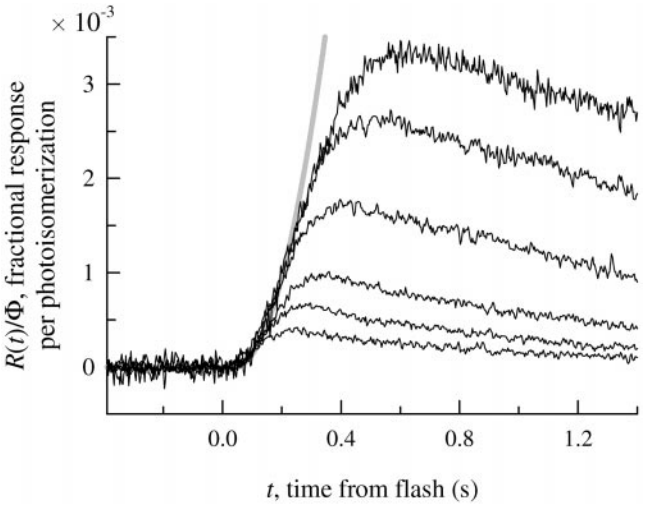

FIGURE 4. Fractional response per photoisomerization, $R(t)/\Phi$, for dim flashes presented in darkness and on five backgrounds, for the rod of Fig. 3 (Table II, rod *b*). In each adaptational state, the mean dim flash response per photoisomerization has been calculated, using only those flash intensities that elicited a relatively small signal; i.e., those with $R(t_{peak}) \leq 30\%$. The traces have broadly the same form as those in Fig. 3 B, but have been averaged from a larger number of trials, and from test flashes of >1 intensity. The background intensities were $I = 0$, 19, 60, 190, 600, and 1,900 photoisomerizations per second, and the respective numbers of flash responses averaged were 51, 37, 30, 30, 43, and 20. The smooth trace (gray) was computed with the pure activation model (Lamb and Pugh, 1992, modified to include the membrane time constant, τ_m according to Equation 5 of Smith and Lamb, 1997), with $A = 0.063\ s^{-2}$, $\tau_m = 20$ ms, and $t_{eff} = 20$ ms.

test thoroughly whether the gain of transduction is altered during light adaptation.

Invariance of the Initial Activation Phase of Phototransduction

To examine this question, it is essential (as explained in THEORY) to express the cGMP-activated currents (and/or responses) in fractional form. Accordingly, Fig. 3 presents results similar to those in Fig. 2, from a rod tested under six different states of adaptation, after transformation in three ways. First, we plotted the fractional cGMP-activated response, $R_{cG}(t) = j_{cG}(t)/j_{cG}(I)$; second, we expanded the time scale by factors of ~10- and 20-fold; and third, we grouped the responses according to flash intensity rather than background. The individual panels in Fig. 3 (A–I) paint a highly consistent picture: for every flash intensity the fractional response $R(t)$ began rising along a common trajectory independent of the state of adaptation.

It might be thought that the common initial rate of rise in Fig. 3 could be limited by the membrane time constant. However, even at the highest flash intensity (Fig. 3 I) the slope was only 12 s^{-1}, well short of the maximal slope (60 s^{-1}) previously reported for responses of nonvoltage-clamped salamander rods stimulated with much more intense flashes, which has been shown to be set by the membrane time constant (Cobbs and Pugh, 1987). Hence, the membrane capacitive time constant will only become limiting at even higher flash intensities than illustrated in Fig. 3.

In the THEORY, we drew the important conclusion from Eq. 6 that the occurrence of a common rising phase for the fractional response $R(t)$ in the presence of different backgrounds could only occur if the initial time course of the underlying PDE activation was common. Applying that insight, we conclude from the analysis of Fig. 3 that a flash of fixed intensity elicits an increment in PDE activity, $\Delta\beta(t)$, which initially is independent of the state of steady adaptation. We applied the same analysis to the responses of the 11 rods for which extensively averaged records were available (Table II), and for two additional rods with less extensive data, for backgrounds suppressing up to 75% of the dark current. In all cases, behavior very similar to that in Fig. 3 was observed, with close coincidence of the early phase of the fractional response $R(t)$ to a given flash presented on different backgrounds.

As a final point in relation to the traces in Fig. 3, it is interesting to note that the more intense the background, the earlier in time the peeling-off occurs; i.e., the earlier the deviation of the fractional response from the common initial trajectory. In a subsequent section, we show that behavior of this kind is, in fact, expected as a consequence of the increased steady rate constant of cGMP hydrolysis, $\beta(I)$, whose measurement we describe shortly.

From the results for the rod in Fig. 3, we calculated the average dim-flash response per photoisomerization, $R(t)/\Phi$, in each of the six adaptational states, and we have plotted these traces in Fig. 4. For each background intensity (or darkness), we considered only those test flash intensities that elicited a fractional response $R(t)$ of less than ~30% at its peak, and we calculated the weighted average response per isomerization. Hence, the composite plot in Fig. 4 is broadly analogous to any of the individual panels for a fixed flash intensity in Fig. 3 (e.g., Fig. 3 D), except that it is constructed only from dim-flash responses and has been scaled according to flash intensity. It is also similar to the plot in Figure 3 of Baylor and Hodgkin (1974) for turtle cones, except that the traces in that plot were not scaled according to the maximal response in each adaptation condition.

Fig. 4 extends our finding of an invariant early rise at any fixed intensity, by showing that the initial time course of the fractional response per photoisomerization $R(t)/\Phi$ is invariant. Furthermore, this figure shows that the parabolic approximation of the "activation only" model provides a remarkably accurate prediction of the response in each adaptational state, up until the

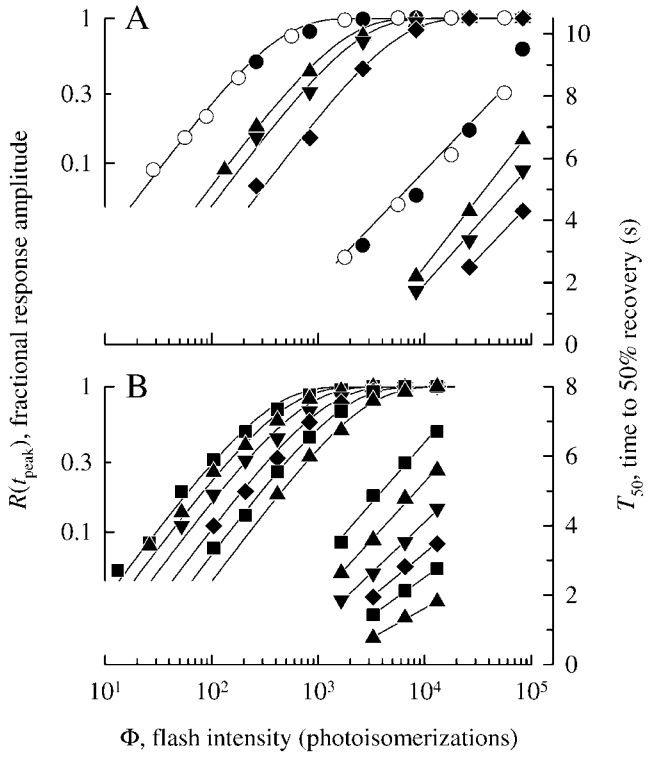

FIGURE 5. Effects of light adaptation on fractional response amplitude and recovery time for saturating flashes. (A) The cell of Fig. 2 (Table II, rod *a*); and (B) the cell of Fig. 3 (Table II, rod *b*). For each cell, a family of responses was obtained for flash intensities ranging from 10 to at least 10,000 photoisomerizations, presented in darkness or on backgrounds of at least three intensities. From these families, two parameters were measured and plotted: (1) the fractional response amplitude, $R(t_{peak}) = r(t_{peak})/j(I)$, measured at the peak, is plotted in the top left of both panels, using the left ordinate scale; and (2) the time to 50% recovery, T_{50}, (for each flash sufficiently bright to saturate the response) is plotted in the bottom right of both panels, using the right ordinate. Each symbol shape represents a different background intensity; closed symbols are for 20 μs xenon flashes; open symbols are for 22 ms flashes from the shuttered beam. (A) ●, ○, darkness; ▲, ▼, and ◆, I = 260, 810, and 2,600 photoisomerizations per second, respectively; (B) ■, darkness; ▲, ▼, ◆, ■, and ▲, I = 19, 60, 190, 600, and 1,900 photoisomerizations per second, respectively, from the top down. All points in the four plots represent averages derived from 2–15 individual responses; error bars have been omitted for clarity. For the points in the recovery half-time plots, the average SDs for the four adaptation conditions of A are 0.15, 0.28, 0.09, and 0.13 s; for the six adaptation conditions of B, they are 0.18, 0.17, 0.13, 0.12, and 0.08 s.

time of peeling off (which is shorter in the presence of brighter backgrounds), at which point each individual experimental trace suddenly deviates from the parabola.

Absolute Sensitivity and Fractional Sensitivity during Light Adaptation

We now illustrate the method described in the THEORY for extracting a measure of flash sensitivity that is "corrected for response compression." Fig. 5, A and B, illustrates data from the rods of Figs. 2 and 3, respectively. The top left section of each panel (left ordinate) plots the amplitude of the rod's fractional response, R (measured at the peak), as a function of flash intensity Φ; the circles were obtained under dark-adapted conditions, while the other sets of symbols correspond to different background intensities. The fractional sensitivity, $S = R/\Phi$ in the limit of dim flashes (see THEORY), is given by the horizontal position of the curves that have been fitted; for the dark-adapted measurements in Fig. 5 A, the horizontal position gives the fractional sensitivity as $S_{Dark} = 0.0036$ photoisomerization^{-1}. (The fitted curves on the leftside of Fig. 5 are exponential saturation functions, but the chosen form of equation is not critical since all that is relevant to sensitivity is the horizontal positioning at dim flash intensities.) For the three backgrounds tested in Fig. 5 A, the rightward shifts of the other fitted curves from the dark-adapted one give the relative fractional sensitivity S_{rel} as 0.24, 0.18, and 0.08. These rightward shifts reflect the extent of desensitization of transduction because of factors other than response compression. We shall return later to the results plotted in the lower right of each panel in Fig. 5.

Collected Measurements of Circulating Current and Sensitivity

In Fig. 6, we summarize our steady-state measurements of circulating current and sensitivity for all the rods of this study as well as for selected results from salamander rods in other investigations; in each panel, the values are given relative to the dark-adapted level. Fig 6. A presents the relative circulating current in the steady state, $J_{rel}(I) = j(I)/j_{Dark}$. Fig. 6 (B and C) present the relative measures of sensitivity, s/s_{Dark} and S/S_{Dark}, where $s = r/\Phi$ is the absolute sensitivity, and $S = R/\Phi$ is the fractional sensitivity, as defined in the THEORY. The relative sensitivity in Fig. 6 B is the parameter that usually has been plotted in previous studies, and the relative fractional sensitivity in Fig. 6 C is obtained by dividing the results in B by those in A (Eq. 8). The values in Fig. 6 C are completely equivalent to the lateral shifts shown for the two illustrative cells on the left of Fig. 5, and represent the reduction in flash sensitivity after correction for response compression. Also shown in Fig. 6 are theoretical traces (continuous curves), which we will describe later.

Measurement of the Steady-state Rate Constant of cGMP Hydrolysis, β(I)

An unavoidable consequence of increasing the intensity of the steady illumination is that the steady rate constant of cGMP hydrolysis β(*I*) will increase, and it is our goal both to measure this increase and to show how it contributes to desensitization. To measure the steady rate constant β(*I*), we used the IBMX-jump method of

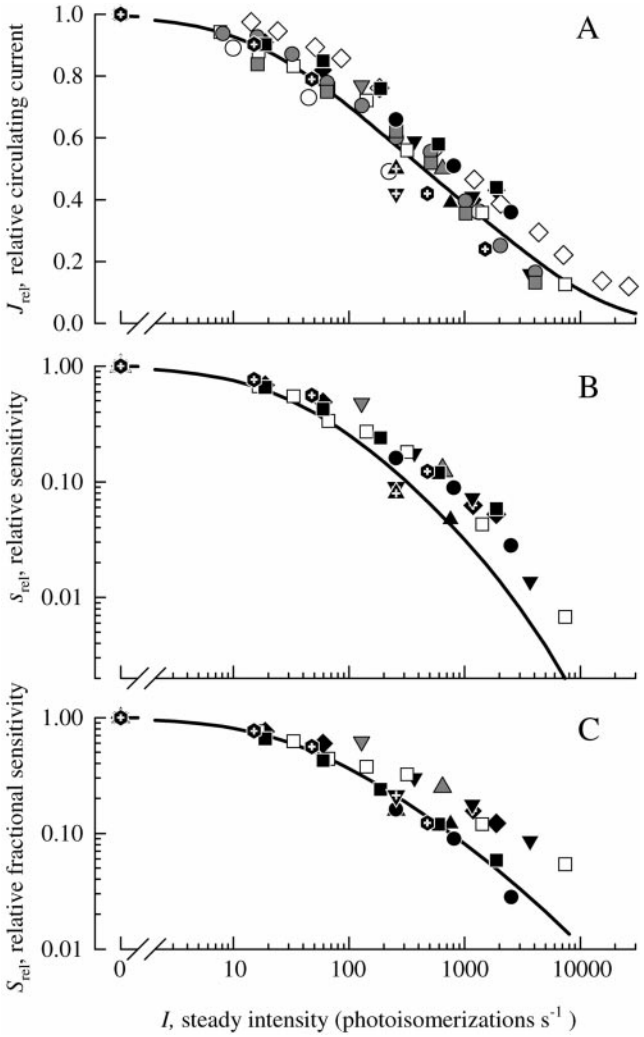

FIGURE 6. Dependence of steady circulating current and flash sensitivity of salamander rods on background intensity. (A) Relative circulating current in the steady state, $J_{rel}(I) = j(I)/j_{Dark}$, where $j(I)$ is the steady current and j_{Dark} is the dark current. (B) Relative sensitivity, defined as $s_{rel}(I) = s(I)/s_{Dark}$, where $s(I)$ is the absolute sensitivity and s_{Dark} is its dark-adapted value. (C) Relative fractional sensitivity, defined as $S_{rel}(I) = (s(I)/s_{Dark})/J_{rel}(I)$; see Eq. 8. Symbols from the present investigation are identified in Table II. Symbols from three previous studies are: ○, Hodgkin and Nunn, 1988; □, Matthews et al. (1988), average of seven cells; ◇, Koutalos et al. (1995b), average of six cells. The curves are the predictions of the model set out in the APPENDICES, using the parameters of the "standard" rod listed in Table IV. The curve in A was obtained from Eq. B7 in Appendix B. The curves in B and C were obtained by simulating (at a range of background intensities) the response to a dim flash, and determining its peak amplitude.

Hodgkin and Nunn (1988) with modified analysis. (We retain the conventional term rate constant to describe β, even though the value of β is not constant, but varies as a function of steady intensity and can also change dynamically during the light response.)

Fig. 7 A superimposes the fractional current recorded in response to seven repetitions of exposure of a dark-adapted rod outer segment to Ringer's solution containing 500 μM IBMX. Once the current had increased appreciably, a saturating flash was delivered (with manual triggering; timing indicated by arrows), and shortly thereafter, the rod was returned to normal Ringer's solution. The responses to IBMX exposure were highly reproducible. Furthermore, no differences were observable between two traces obtained in total darkness and five traces obtained in the presence of the normal dim infrared illumination. These seven responses are shown again in Fig. 7 B on a faster time base (lowest set of traces), along with similar results collected when the rod had adapted to steady backgrounds of three intensities. In each case, the current was expressed as the fraction $J(t)$ of the steady-state level before IBMX exposure.

Our first method of estimating $\beta(I)$, which is closely similar to that of Hodgkin and Nunn (1988), is illustrated in Fig. 7 C. It is based on the assumption that a few hundred milliseconds after the solution change, the IBMX concentration within the outer segment will have risen enough to totally inhibit all the PDE activity, yet the cyclase rate $\alpha(t)$ will not have changed from its initial steady rate $\alpha(I)$. On the basis of the first of these assumptions, the term β in Eq. A3 disappears, so that $dcG/dt \approx \alpha(t)$, whereas on the basis of the second assumption, $\alpha(t) \approx \alpha(I) = \beta(I)\ cG(I)$, so that in conjunction with Eq. 4 we can write

$$\beta(I) \approx \frac{d}{dt} J_{cG}(t)^{\frac{1}{n_{cG}}}. \quad (9)$$

One difference between this formulation and that of Hodgkin and Nunn (1988) is that we use normalization with respect to the steady current present before the IBMX exposure, rather than with respect to the dark current.

As assumed by Hodgkin and Nunn (1988), we ignore the exchange current (i.e., we assume that $j_{cG} \approx j_{tot}$), and we take the maximum value of the derivative, which occurs ~100–200 ms after the solution change, to represent $\beta(I)$. Thus, an implicit assumption of this method is that the time of occurrence of the maximal slope is late enough that the IBMX will have equilibrated, but early enough that the cyclase rate will not have changed. Accordingly, the peaks of the traces plotted in Fig. 7 C provide estimates of the steady rate constant of cGMP hydrolysis applicable in darkness and in the presence of steady adapting backgrounds. We hypothesize that the main limitation in this approach is that α is not constant after the solution change and, instead, that the increase in Ca^{2+} concentration that occurs within 200 ms can cause appreciable inhibition of guanylyl cyclase before maximal inhibition of PDE occurs, thus, leading to underestimation of the rate constant, $\beta(I)$.

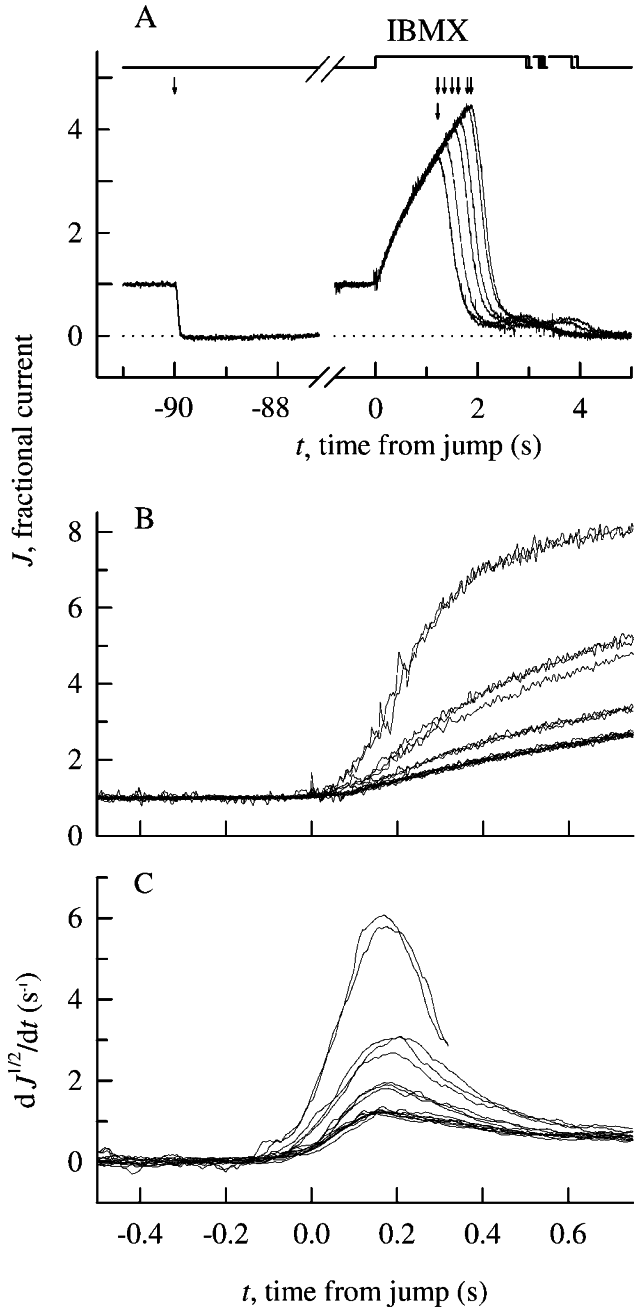

FIGURE 7. Method of estimation of the steady-state PDE rate constant of cGMP hydrolysis. (A) Exposure to 500 μM IBMX, on a slow time-base, showing seven repeated trials under dark-adapted conditions. In A and B, the fractional circulating current, $J(t) = j(t)/j(I)$, has been plotted, determined by the following protocol. The steady circulating current $j(I)$ was measured, by delivering an intense flash (Φ = 8,600 photoisomerizations) at the first arrow. For this rod, we obtained j_{Dark} = 34 pA under the dark-adapted conditions of A. After a delay of 90 s, to allow complete recovery, a rapid translation of the chamber moved the laminar boundary of the flowing solutions across the rod (defined as time zero), exposing the outer segment to Ringer's solution containing 500 μM IBMX, and eliciting a rapid increase in circulating current because of inhibition of phosphodiesterase activity. A flash of the same intensity as before was then delivered under manual control (arrows), and ~1 s later the rod was returned to control Ringer's solution. The rod was allowed to recover for several minutes, and the IBMX exposure and flash were repeated for a total of seven times. After the series of jumps, the response amplitude was again measured, and found to be 32.5 pA. Two of the seven records were obtained in the absence of infrared illumination, and are indistinguishable from the other five. The small "bumps" in the response tails occur at the time of return to control Ringer's solution, and are due to the extrusion of Ca^{2+} by the Na^+/Ca^{2+}-K^+ exchanger. (B) Fractional circulating current $J(t)$ on a faster time-base, for jumps into IBMX in the dark, or in the presence of steady illumination producing I = 15, 48, or 480 photoisomerizations per second, that reduced the relative circulating current to $J_{rel}(I)$ = 0.90, 0.79, and 0.42 (n = 7, 3, 3, and 2 traces, respectively). The traces in darkness are the same as in A. (C) Derivatives of $J(t)^{1/2}$, estimated by fitting each trace with a running 61-point parabola, and evaluating the derivative at the midpoint. At the sampling rate of 300 Hz, this parabola covered 0.10 s before and after the midpoint; the apparent rise of the derivatives before time zero is an artifact of using this finite width. Derivatives estimated with narrower windows gave similar maxima, but greater noise. Rod *d* of Table II.

In an attempt to investigate this hypothesis, we numerically integrated the entire set of equations for phototransduction presented in APPENDIX A, as described in detail in MATERIALS AND METHODS (see Tables III and IV).

Fig. 8 compares the recorded responses to IBMX steps with the predictions of the model, for two cells: the top row (Fig. 8, A and B) shows the averaged traces from Fig. 7 B, whereas the bottom row (Fig. 8, C and D) shows similar averaged traces from the rod of Fig. 2. The left and right columns show the predictions obtained using two assumptions for the value of the Hill coefficient of the cGMP-activated channels, n_{cG} = 2 (left) and n_{cG} = 3 (right). Inspection of Fig. 8 shows that the quality of fit of the simulated traces to the experimental traces was very good over the initial 200 ms, for each adaptational state, and this finding lends credence to the general adequacy of the theoretical framework laid out in the APPENDICES. Comparison of the left and right columns of Fig. 8 shows that the quality of fit was essentially unaffected by the assumed value of channel cooperativity, n_{cG}. Between the different traces, we kept all the parameters of the model (i.e., those listed in Table IV [see APPENDIX A]) constant, and we varied only the intensity (I) of steady illumination to find the best fit over the initial 200 ms. Even though the fitting has been constrained only over this early phase, the theory traces generated with the model provide a reasonably good general description of the whole family of responses out to 1 s.

The estimates of $\beta(I)$ obtained by the approach illustrated in Fig. 8 coincided closely with those obtained by the derivative method of Fig. 7, for IBMX jumps in darkness and in the presence of relatively dim back-

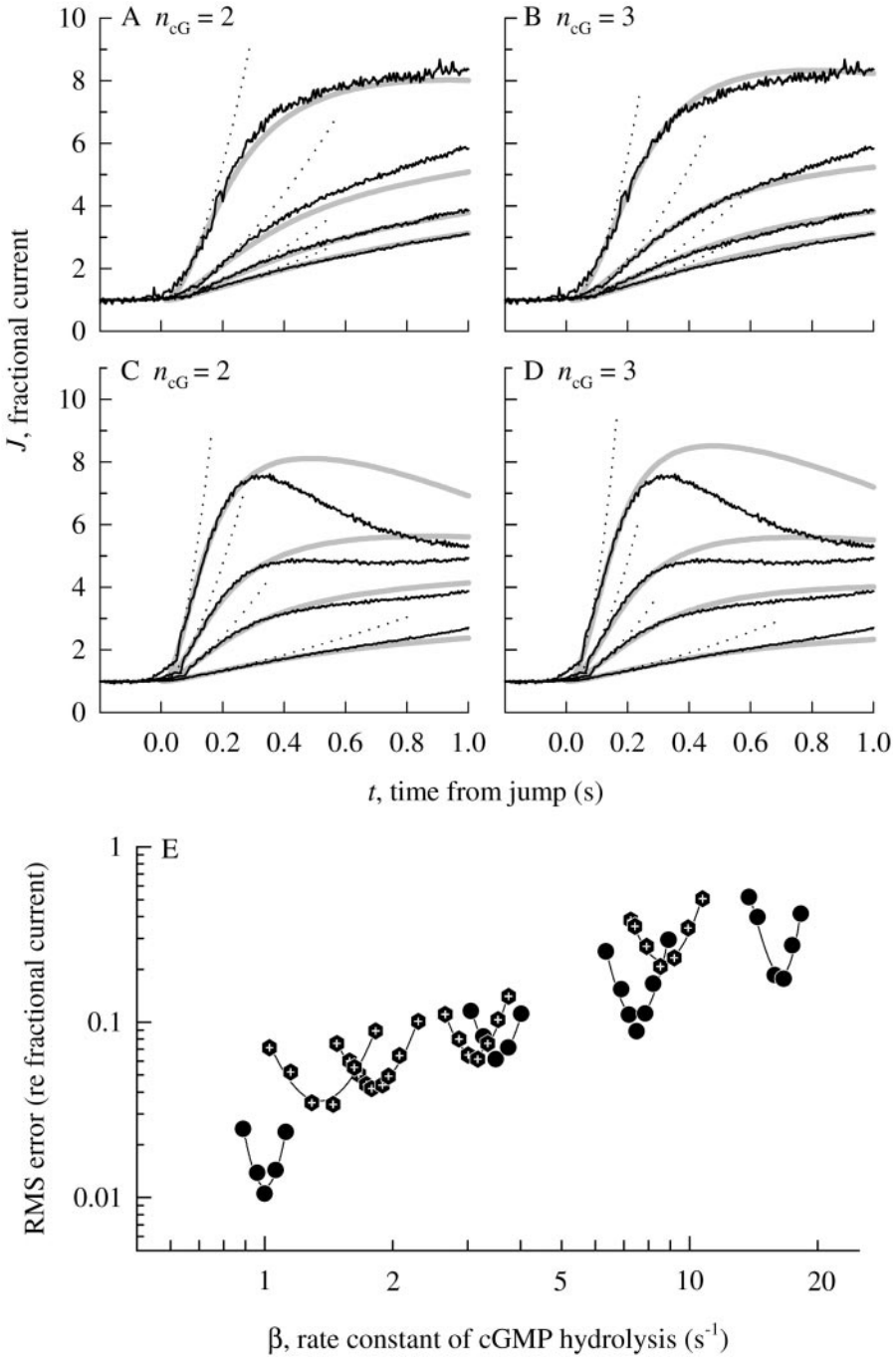

FIGURE 8. Estimation of the steady rate constant $\beta(I)$ of cGMP turnover, by the fitting of simulated responses to the IBMX-jump experiments. The top row (A and B) presents the averaged traces from Fig. 7 B (Table II, rod *d*); the middle row (C and D) presents equivalent results from the rod of Fig. 2 (Table II, rod *a*). The left and right columns show simulations for n_{cG} = 2 and 3, respectively. The procedure for fitting is described in the MATERIALS AND METHODS. In brief, the response of the model in the APPENDICES was evaluated, in response to a sudden reduction in PDE activity from its initial steady level. This calculation was repeated over a range of values of steady intensity (I) to find the intensity and, hence, the value of $\beta(I)$, that minimized the sum-of-squares error from each experimental trace over the time window 0–200 ms. The parameters of the model were set to those measured for the respective cells (Table II, rods *d* and *a*), together with the remaining parameters for the "standard" rod in Table IV (except that Rec_{tot} was set to 20 μM for rod *a*, in C and D). The value of β_{Dark} in each panel was determined by applying the above fitting to the IBMX-jump data obtained under dark-adapted conditions. The dotted curves show the predictions of the model when the Ca^{2+} concentration was clamped at the level predicted by the model for the respective light-adapted state; these curves are well approximated by $J(t) \approx (1 + \beta(I)\,t)^{n_{cG}}$. (E) Dependence of the RMS error on $\beta(I)$, for the two cells, calculated with n_{cG} = 2, denoted with the same symbols as in Table II: ●, for A; ✪, for C. This plot gives an indication of the precision with which $\beta(I)$ is determined by this method.

grounds. However, at brighter backgrounds, the estimates from the derivative method were smaller, as would be expected if that method was compromised by a rapid change in α. Thus, for the cell illustrated in Fig. 8 A, the derivative method gave values of $\beta(I)$ = 1.3, 2.0, 3.2, and 6.6 s^{-1} (in darkness and on the three backgrounds), whereas the simulation approach gave $\beta(I)$ = 1.4, 1.8, 3.2, and 8.5 s^{-1} (in both cases using n_{cG} = 2). Similarly, for the rod of Fig. 8 B, the derivative method gave 0.92, 3.5, 6.6, and 11.5 s^{-1}, whereas the simulation approach gave 1.0, 3.5, 7.5, and 16.6 s^{-1}. We would emphasize that the discrepancy between the pairs of estimates of $\beta(I)$ at higher intensities was not caused by failure of the theory curves to describe the experimental recordings. Indeed, the maximum slopes of the respective experimental and simulated traces agreed closely with each other. Instead, the simulations indicated that, by the time that the maximal slope was attained (150–200 ms), $\alpha(t)$ had declined to ~70% of its initial steady level $\alpha(I)$, so that the approximation underlying Eq. 9 was compromised. Hence, we conclude that the derivative method underestimates $\beta(I)$ at

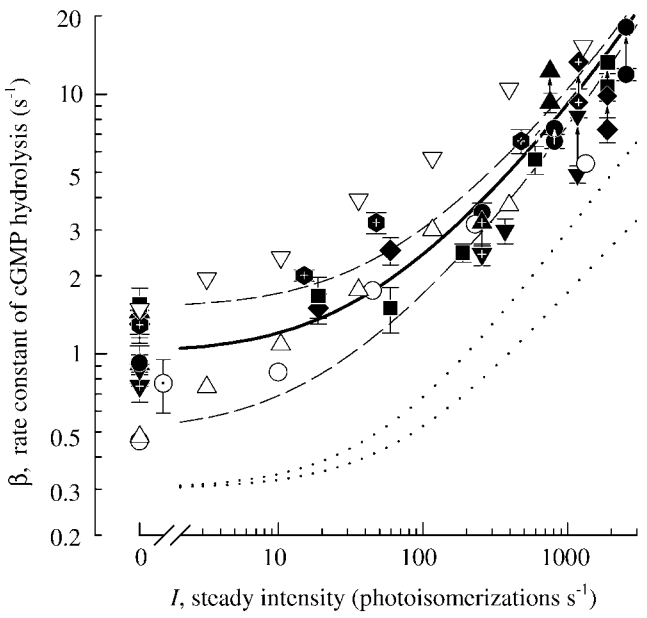

FIGURE 9. Steady-state rate constant, $\beta(I)$, of cGMP hydrolysis as a function of background intensity. (A) Estimates of $\beta(I)$ obtained using the derivative method of Fig. 7 and Eq. 9 are plotted (mean ± SD of repeated measurements). In addition, estimates obtained by the "fitting" method of Fig. 8 are also shown at intensities of $I >$ 800 photoisomerizations per second, linked by vertical arrows to the corresponding points obtained with the derivative method. In all cases, it has been assumed that $n_{cG} = 2$. Closed symbols are from our own experiments and are identified in Table II. Open symbols are from two other studies that used the IBMX-jump or Li^+-jump methods. ⊙, Hodgkin and Nunn (1988) Li^+-jump experiments: single cell from their Figure 2, plus β_{Dark} from Table I, with mean ± SD for $n = 17$ rods. ▽, Cornwall and Fain (1994) IBMX-jump for a single cell, their Figure 6. △, Cornwall and Fain (1994) Li^+-jump for a single rod, their Figure 2. Cornwall and Fain assumed $n_{cG} = 3$ in their analysis, and we have adjusted their data for $n_{cG} = 2$. The solid curve plots the steady-state expression for $\beta(I)$ as a function of I given by Eq. B7, with $\beta_{Dark} = 1.0\ s^{-1}$, $A = 0.08\ s^{-2}$, $n_{cG} = 2$, $\tau_E = 1.6$ s, and $k_{R,max} = 12\ s^{-1}$ (which yields $\tau_{R,\,Dark} = 0.35$ s). The two dashed curves are the same, except for $\beta_{Dark} = 0.5$ and $1.5\ s^{-1}$. The two dotted curves were derived with Eqs. 2–6 of Koutalos et al. (1995b) for $Ca^{2+}_{i,\,Dark} = 200$ nM (bottom dotted trace) and 500 nM (top dotted trace).

higher intensities, and that for these backgrounds, the method of fitting simulated responses is more accurate.

It is possible to investigate this conclusion, and the underlying basis of the effect, by considering the predicted behavior of our model rod to a step of IBMX when changes in Ca^{2+} concentration are prevented. These simulations gave predicted responses (dotted traces in Fig. 8) that followed purely accelerating trajectories. When we compared the maximal slope predicted by the full model with the slope at the corresponding time predicted by the calcium-clamped model, we found only a slight difference in darkness or with a dim background, but a considerable discrepancy when the background was bright. On the assumption that such differences in the model calculations genuinely reflect the behavior of real rods, we conclude that the primary shortcoming in the derivative approach stems from the dynamic change in Ca^{2+} concentration that accompanies exposure to IBMX.

A more intuitive (and less model-dependent) way to arrive at the same conclusion can be obtained by considering a straightforward approximation. If we take the cyclase activity under calcium-clamped conditions to be constant at the steady-state level determined by the background, and then integrate both sides of Eq. 9, we obtain an analytical prediction for the IBMX-jump response as $J(t) \approx [1 + \beta(I)\,t]^{n_{cG}}$. This is a continually accelerating function of time that closely approximates each of the dotted traces in Fig. 8. Importantly, it is the trajectory that the response of the real rod would need to follow, if the derivative method of Eq. 9 were to give the correct value for $\beta(I)$. And since the slope of the real rod's response is considerably smaller than the slope of this trajectory for brighter backgrounds, we again conclude that the derivative method underestimates $\beta(I)$.

Collected Measurements of the Rate Constant of cGMP Hydrolysis, β(I)

We now summarize in Fig. 9 the estimates of $\beta(I)$ obtained with the derivative method (Eq. 9), both from this study (closed symbols) and from previous investigations (open symbols). All estimates were obtained with an assumed Hill coefficient of $n_{cG} = 2$, and to a good approximation the equivalent values for $n_{cG} = 3$ can be obtained simply by scaling all the points down to two thirds of their plotted values. In addition, at the higher intensities, we have also shown the estimates of $\beta(I)$ determined by the fitting method of Fig. 8. Each of these estimates is shown at the upper end of a vertical arrow from the corresponding point obtained with the derivative method, which, as explained above, is expected to provide an underestimate of the true value of $\beta(I)$. The results in Fig. 9 show that, for an assumed channel cooperativity of $n_{cG} = 2$, the estimate of $\beta(I)$ increases from ~1 s^{-1} in darkness to 10–20 s^{-1} for steady illumination of 1,000–2,000 photoisomerizations per second, which (as shown by Fig. 6) suppresses 60–70% of the circulating current. We have intentionally not normalized $\beta(I)$ to its dark level, for reasons that will become apparent later.

In subsequent sections, we will investigate the contribution of this increase in $\beta(I)$ to the desensitization of the flash response observed during light adaptation, and we will also investigate the role that it plays in the earlier "peeling away" of the flash responses from the common initial trajectory, which is observed with more intense backgrounds. But before doing so, we need to quantify any adaptational changes that occur in the other two major recovery processes: the mean lifetime of activated rhodopsin (τ_R) and the mean lifetime of activated PDE (τ_E).

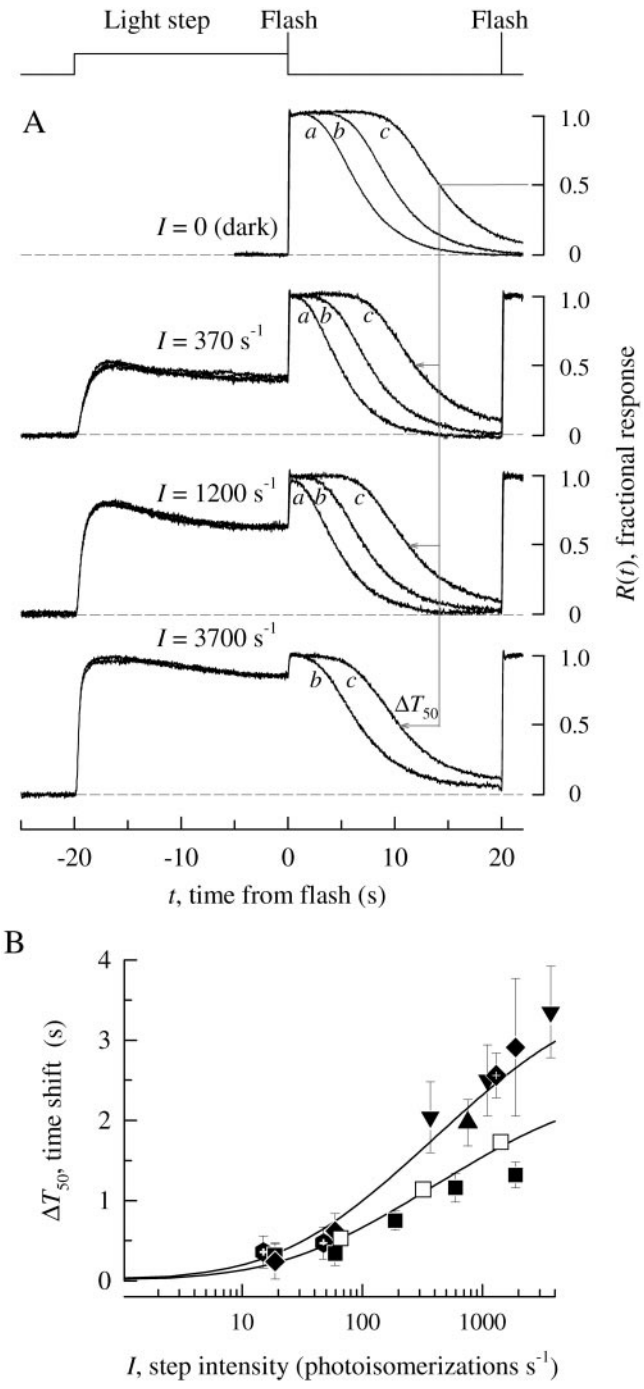

FIGURE 10. Step/flash experiment used as the basis for determining the decrease in R* lifetime. (A) Responses of rod *f* of Table II, stimulated with flashes producing Φ = 5,100 (*a*), 16,000 (*b*), or 51,000 (*c*) photoisomerizations, either in darkness (top set), or synchronously with the termination of a step of light delivering I = 370, 1,200, or 3,700 photoisomerizations per second, that had been applied for 20 s. The effect of the backgrounds in shortening the duration of the response is indicated diagrammatically for flash *c* by the leftward pointing arrows, which originate from a line coinciding with the time of 50% recovery for the flash delivered in darkness; the magnitude of this leftward shift in time to 50% recovery is denoted ΔT_{50}. (The traces were digitally filtered at 50 Hz with the Matlab™ routine "filtfilt".) (B) Dependence of ΔT_{50} on step intensity for six rods from this study (closed symbols, identified in Table II), and for the rod in Figure 8 of Fain et al. (1989), □, which was exposed to steps lasting 7 s. When more than 1 flash intensity was used (as in A), ΔT_{50} was determined as the mean shift for the different intensities, and the bars indicate ± SD. The two curves plot predictions of the model in the APPENDICES using the parameters of the standard rod, except for τ_E, which is 2.4 s for the top curve and 1.6 s for the bottom curve.

The Mean Effective Lifetime of Activated PDE during Light Adaptation

Previous investigations have shown that the "dominant" time constant in recovery of the bright-flash response (i.e., the slowest time constant) is virtually unaffected by light adaptation or by cytoplasmic Ca^{2+} concentration (Pepperberg et al., 1992, 1996; Lyubarsky et al., 1996; Murnick and Lamb, 1996; Nikonov et al., 1998). Nikonov et al. (1998) have reviewed the evidence and concluded that this time constant corresponds to the mean lifetime of activated PDE, denoted as τ_E.

The method for estimating the magnitude of the dominant time constant is illustrated by the points in the bottom right section of the two panels in Fig. 5. The measurements plot the time taken for recovery to a criterion level of circulating current (of 50% in Fig. 5) after saturating flashes of different intensity, which were presented either in dark- or light-adapted conditions. When the flash intensity is plotted on a logarithmic scale, as in Fig. 5, then a straight line relationship is consistent with first-order removal of a substance that is produced in proportion to light, and the slope of this line is directly proportional to the time constant of removal. Hence, the straight, and broadly parallel, results in Fig. 5 A are consistent with first-order removal, with a time constant that appears independent of adapting intensity (1.6 ± 0.2 s, mean ± SD). In Fig. 5 B, the points at each background fall along a straight line, but the slope of the line appears to decline as the background intensity increases, indicating a reduction in the size of the dominant time constant at higher levels of adaptation. Our collected measurements are presented in Fig. 11, and will be described shortly.

Measurement of the Effective R Lifetime during Light Adaptation*

Fig. 10 illustrates an experiment of a type introduced by Fain et al. (1989) that has been hypothesized to measure the change in effective lifetime of R* elicited by adaptation to backgrounds (Matthews, 1996, 1997; Murnick and Lamb, 1996). The protocol, which we refer to as a "step/flash" experiment, is illustrated in Fig. 10 A. The rod was exposed to a saturating flash, either in darkness (top set), or synchronously with the extinction

of a background that had been applied for 20 s (bottom sets). In this particular experiment, three different intensities of saturating flash were used (indicated by *a*, *b*, and *c*), in conjunction with backgrounds delivering I = 0, 370, 1,200, or 3,700 photoisomerizations per second.

As reported by Fain et al. (1989), recovery of the saturating response to any criterion level is accelerated when the flash is preceded by background illumination. For the brightest flash (*c*) in Fig. 10 A, the extent of this step/flash acceleration is illustrated graphically by the horizontal arrows that have been drawn from the vertical line that marks the time to 50% recovery in the absence of any preceding exposure to a background. In this case, the shifts for the three backgrounds were measured as ΔT_{50} = 2.3, 2.9, and 3.7 s, where the symbol ΔT_{50} denotes the shortening of recovery time measured at the 50% criterion level.

By examining the other test flash intensities, and other criterion levels of recovery, we found that the measurements of step/flash acceleration were quite robust. For the intermediate flash intensity (*b*), the corresponding shifts for the three levels of adaptation were ΔT_{50} = 2.1, 2.5, and 3.0 s, broadly comparable to (but 10–18% shorter than) the values obtained with the strongest flash. Similarly, at a criterion level of 20% recovery, the shifts were ΔT_{20} = 2.0, 2.6, and 3.1 s for flash *b*, and 2.3, 3.0 and 4.0 s for flash *c*. The relatively small size of the variations indicates that the shape of the recovery phase is similar at different intensities of saturating flash, but simply shifted in time, and that the dominant time constant of recovery is at most only weakly affected by background illumination. In the following analysis we will neglect such variations. Fig. 10 B presents the shift ΔT_{50} as a function of adapting intensity, for six rods from this study and for the rod in Fain et al. (1989) Figure 8. The theory traces in Fig. 10 B will be described shortly.

By making several assumptions, it is possible to convert the shifts obtained in the step/flash experiments into changes in the effective lifetime of R*. The first two assumptions are expressed in Eqs. A1 and A2 of Appendix A, which specify that the activities of R* and E* each decline as first-order processes, with time constants τ_R and τ_E at a given level of adaptation. The third assumption is that τ_E is independent of background intensity, a matter that we examine in Fig. 11. The final assumption is that $\tau_E > \tau_R$. This last assumption restates our view, set out in the previous section, that τ_E represents the dominant time constant of recovery, and can therefore be estimated from the slope of the plot of recovery time versus logarithm of flash intensity, of the kind illustrated in Fig. 5.

The practical meaning of these assumptions is that, when measured at times much greater than τ_R, the state of activation underlying the saturating flash response declines as an exponential with time constant τ_E, from

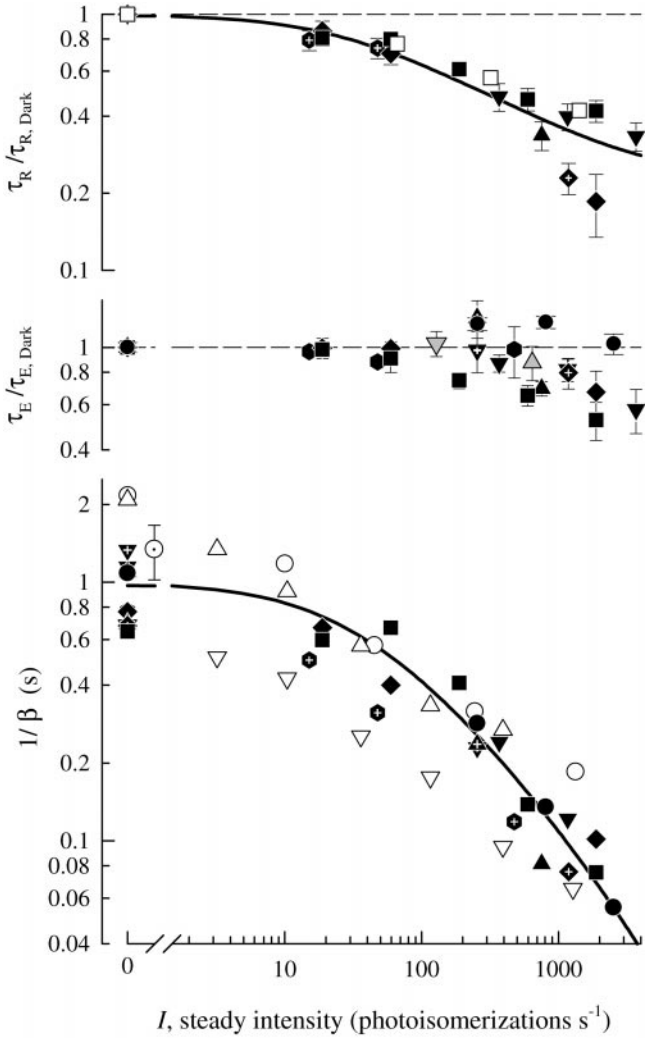

Figure 11. Dependence of the three main time constants of rod phototransduction on the intensity of steady adapting light. (A) $\tau_R/\tau_{R,\,Dark}$, the effective lifetime of R* relative to its dark-adapted lifetime, inferred as described in the text (Eq. 10) from the step/flash experiments of Fig. 10. (B) $\tau_E/\tau_{E,\,Dark}$, the effective lifetime of activated PDE, E*, relative to its dark-adapted lifetime, extracted by measuring the dominant time constant of recovery for saturating flashes (Fig. 5). (C) Time constant of cGMP hydrolysis, $1/\beta(I)$, determined as the reciprocal of the steady-state rate constant of hydrolysis as measured by the methods of Figs. 7 and 8, and summarized in Fig. 9. The error bars (Fig. 9) have been removed for simplicity, and only the estimates obtained with the fitting method (Fig. 8) have been shown in cases in which the two methods yielded different estimates of β.

an initial level that is directly proportional to the time constant τ_R. Hence, if τ_R changes from its dark-adapted value of $\tau_{R,\,Dark}$ then the induced shift in recovery time ΔT is given to a good approximation by the exponential relation

$$\frac{\tau_R}{\tau_{R,\,Dark}} \equiv \frac{k_{R,\,Dark}}{k_R} \approx \exp\left[-\frac{\Delta T}{\tau_E}\right]. \qquad (10)$$

Analysis of the exact form of the solution to Eqs. A1 and A2, given by Nikonov et al. (1998), shows that the ap-

proximation involved in Eq. 10 is very accurate when τ_E is much greater than $\tau_{R,\,Dark}$, as is the case in the salamander rod, where τ_E = 1.5–2.7 s and $\tau_{R,\,Dark} \approx 0.4$ s, and we therefore adopt Eq. 10 in the estimation of τ_R. The extracted values are presented in the next section along with those of the other two time constants of recovery.

It is worth mentioning that, even if the assumption of first-order decline in R* activity is not correct, the ratio calculated in Eq. 10 (and plotted in Fig. 11 A) remains useful. Provided that the R* activity declines much more rapidly than the PDE time constant τ_E, the factor $\exp(-\Delta T/\tau_E)$ will represent the light- to dark-adapted ratio of the integrated R* activity, $\int R^*(t)\,dt$.

To compare the shifts measured in the step/flash experiments with theory, we include in Fig. 10 B two traces generated with our model of recoverin's interaction with RK. The traces were generated by solving the steady state, including the equations of APPENDIX C, and then substituting the values of $\tau_R(I)/\tau_{R,Dark}$ from Eq. A12 into Eq. 10 above to obtain ΔT. We used two values of τ_E corresponding roughly to the upper and lower range of estimates obtained in Table II: τ_E = 2.4 s (Fig. 10 A, top trace) and 1.6 s (Fig. 10 A, bottom trace). Comparison of these traces with the symbols in Fig. 10 B shows a general correspondence between the predicted shifts and the estimates of τ_E (Table II). Thus, rod *f* (▼, τ_E = 2.7 s) exhibited the largest shifts, whereas rod *b* (■, τ_E = 1.5 s) exhibited the smallest.

Dependence of the Three Principal Time Constants of Recovery on Adaptation Level

In Fig. 11, we present our collected measurements of the three principal time constants governing the recovery phase of salamander rod phototransduction as functions of the intensity *I* of steady background illumination. The estimated lifetimes of R* and E* have been plotted relative to their dark-adapted levels, as $\tau_R/\tau_{R,\,Dark}$ (A) and $\tau_E/\tau_{E,\,Dark}$ (B). But, for the lifetime of cGMP (C), we plotted $1/\beta$ without normalization to the dark-adapted level. Our reason for not doing so is that β_{Dark} appeared to vary from cell to cell in a manner unrelated to the light-activated PDE activity. Thus, in Fig. 9, β_{Dark} exhibited a range of nearly fourfold, whereas at backgrounds in the neighborhood of I = 1,000 photoisomerizations per second, the range of $\beta(I)$ was only slightly greater than twofold.

Fig. 11 B shows that the E* lifetime τ_E is at most only weakly dependent on background intensity, with the estimates for most rods decreasing by 20–40% for backgrounds producing >500 photoisomerizations per second (see also Fig. 5 B). We are uncertain whether this apparent decline in τ_E is a true reflection of an underlying mechanism or whether it is due in some way to the limitations of the method of analysis.

In contrast to the modest and somewhat irregular decline in the estimate of τ_E, all rods exhibited a systematic decline in the estimate of τ_R beginning at the lowest backgrounds and reaching three- to fivefold at the highest backgrounds. One of the assumptions underlying the calculation of $\tau_R/\tau_{R,\,Dark}$ is that τ_E is independent of background intensity, and, as discussed above in relation to Fig. 11 B, this assumption may not be strictly correct. If the time constant τ_E does decrease with increasing background intensity then the values of $\tau_R/\tau_{R,\,Dark}$ that we have extracted will be underestimates; i.e., the true reduction in τ_R will not be as pronounced as suggested by Fig. 11 A. The curve in Fig. 11 A plots the predictions of a model of recoverin's calcium-dependent inhibition of rhodopsin kinase that will be considered in the DISCUSSION and APPENDIX C.

In comparison with the modest changes shown in Fig. 11 (A and B), the reduction in the time constant of cGMP turnover, $1/\beta$ that is plotted in Fig. 11 C is much greater, declining by ~20-fold at backgrounds of 2,000 photoisomerizations per second. Hence, for the three inactivation reactions of phototransduction, the crucial message of Fig. 11 is that, in the transition from dark- to light-adapted conditions, the change in the mean lifetime is modest for R*, small for E*, and major for cGMP.

Significance of the Altered Time Constants

To assess the effects of the changes in the time constant on response kinetics and flash sensitivity, Fig. 12 presents the responses of the rod of Fig. 2 (Table II, rod *a*), along with theoretical traces computed using the model set out in the APPENDICES. The responses have been normalized in the manner of Fig. 3. Thus, we plotted the fractional cGMP-activated current $J_{cG}(t) = j_{cG}(t)/j_{cG}(I)$ according to Eq. 5, which assumes that the component j_{ex} of Na^+/Ca^{2+}-K^+ exchange current does not change appreciably over this time scale (Fig. 2). To concentrate on the steady-state effects induced by the backgrounds, rather than on any dynamic changes elicited by the test flashes, we have restricted examination to the first 250 ms after the flash. And likewise, to concentrate on the steady state rather than dynamic predictions of the model, the theoretical traces have been computed under calcium-clamp conditions. Thus, the steady state of the model has been computed as described in APPENDIX B, to generate the parameters $Ca(I)$, $\tau_R(I)$, $\beta(I)$, etc., and thereafter the simulated flash response has been computed with $Ca(t)$ held at $Ca(I)$. This is equivalent to an experiment in which the rod first adapts to a background in Ringer's, and is then exposed to a calcium-clamping solution, during which period it is tested with flashes.

Comparison of the experimental and theoretical traces in Fig. 12 (A–D) shows that, on the whole, the model provides a good account of the early phase of each family of flash responses. To assist in evaluating the significance of the steady-state changes, we present two additional panels (Fig. 12, E and F). Fig. 12 E superimposes all the traces presented in A–D, reconfirming that (irrespective of background intensity) the frac-

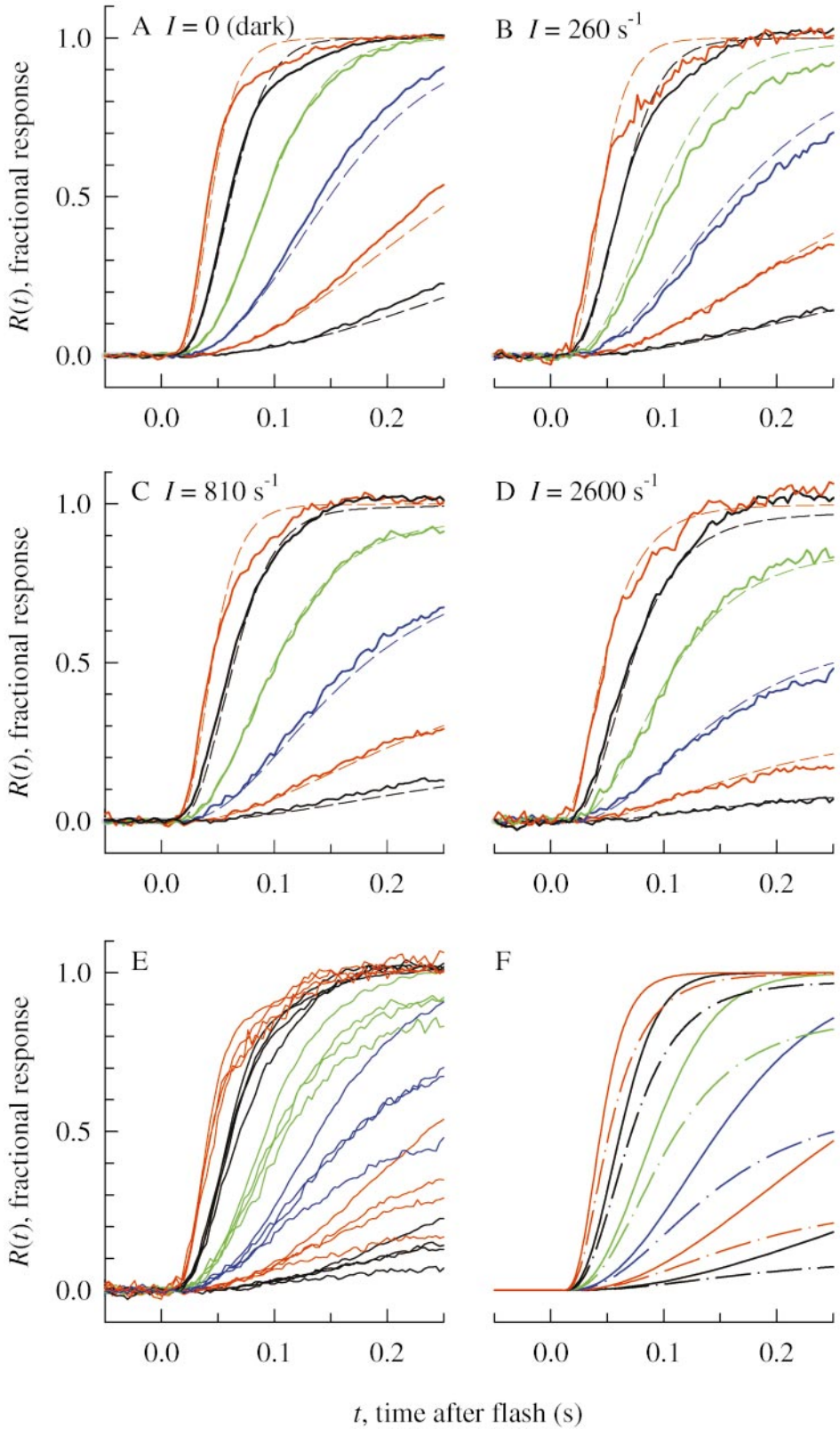

FIGURE 12. Comparison between experiment and theory, for fractional responses $R(t)$ to families of flashes presented in darkness or on backgrounds. Same cell and traces as in Fig. 2 (rod *a* of Table II). A–D each depict responses to the same set of flash intensities, but presented on steady backgrounds delivering I = 0 (A), 260 (B), 810 (C), or 2,600 (D) photoisomerizations per second. Each set of raw responses has been normalized by the saturating response amplitude at 200–250 ms for that background condition (see Fig. 2), to extract the fractional response. In each adaptation condition the flashes delivered Φ = 260, 830, 2,600, 8,300, 26,000, 83,000 and 260,000 photoisomerizations. The smooth traces were computed with the model in the APPENDICES, under calcium-clamp conditions; i.e., with Ca^{2+}_i held at the level calculated for each steady background. The parameters of the model were those for the standard rod, given in Table IV (including the value of β_{Dark} = 1.0 s, which was measured for the individual rod, see Table II). In the presence of the three backgrounds, the model gave the following steady state values: $\beta(I)$ = 3.2, 6.7, and 15.9 s^{-1}; $\tau_R(I)$ = 0.26, 0.21, and 0.18 s. (E) All the traces from A–D have been superimposed, with the same color-coding according to flash intensity as in the individual panels. (F) The theory traces from A (dark-adapted, solid lines) and D (the brightest background, dashed lines) are superimposed to illustrate the predicted differences for calcium-clamped responses between the two extremes of adaptation.

tional responses to each flash intensity do indeed begin rising along a common trajectory; however, they peel off earlier as the background intensity increases. Likewise, Fig. 12 F superimposes the theoretical traces from A and D, emphasizing the extent of change in predicted kinetics between the two extreme states of adaptation: dark-adapted (continuous traces), and on a background of 2,600 photoisomerizations per second (dashed traces). Since we have eliminated any dynamic (i.e., flash-induced) change in parameters from these

simulations, and since the steady-state changes in cyclase activity are accounted for in the procedure of normalization to fractional cGMP-activated current, we conclude that the peeling-off behavior observed in the simulations on this time scale is mediated entirely by steady-state changes in $\beta(I)$ and $\tau_R(I)$.

To further assess the effects of altered $\beta(I)$ and $\tau_R(I)$ on response kinetics and sensitivity, we reexamined previous experimental work in which $Ca^{2+}{}_i$ was clamped after adaptation to background illumination. The results from Figure 10 B of Fain et al. (1989) are replotted here in Fig. 13 (noisy traces) and are compared with the predictions of our equations (smooth traces). In their experiment, dim flashes were delivered during exposure to calcium-clamping solution that was presented after the rod had equilibrated either to darkness (Fig. 13 A) or to a background of 96 (Fig. 13 B) or 2,100 photoisomerizations per second (Fig. 13 C). The theory traces are simulations obtained as described above, with $Ca^{2+}{}_i$ clamped to the level determined by the steady-state solution for the three cases, i.e., darkness, 580 nM; dimmer background, 400 nM; and brighter background, 150 nM (see legend for details).

We think it impressive that the general form of agreement between simulation and experiment is so close under these conditions of calcium clamp. In considering this behavior, it is important to note that the pronounced acceleration of response kinetics in the presence of the background occurs in spite of the prevention of dynamic (i.e., response-induced) changes in $Ca^{2+}{}_i$, both in experiment and simulation. Thus, the time to the peak of the experimental responses decreases from 2.4 s in darkness (Fig. 13 A) to 1.2 s on the dimmer background (Fig. 13 B) and to 0.7 s on the brighter background (Fig. 13 C), purely as a result of steady-state changes in transduction parameters. Less obvious in Fig. 13, but equally important, is the fact that the fractional sensitivity of the response also declines, despite the clamping of $Ca^{2+}{}_i$ to its steady level. To appreciate this desensitization, it is necessary to note that the test flash intensity increased in the ratio 1:4:25 in the three panels of Fig. 13; measurement of the peak amplitudes indicates that the relative fractional sensitivity $S_{rel}(I)$ (defined in Eq. 8) declined in the ratio 1:0.23:0.027.

The effects of the decline in the time constants $\tau_R(I)$ and $1/\beta(I)$ on fractional sensitivity and kinetics can be approximated by the convolution of three first-order decay reactions, where two of the time constants change with adaptation while τ_E remains constant. This corresponds closely to one formulation of the effects of adaptation considered by Baylor and Hodgkin (1974) for turtle cones, except that only three time constants are involved here, and each is explicitly identified with a molecular step in the phototransduction cascade. As in the analysis of Baylor and Hodgkin (1974), a background-induced reduction in the time constants of inactivation reactions leads to desensitization and acceleration of recovery kinetics. We will examine this matter further in the DISCUSSION, in the context of considering all the factors contributing to desensitization.

DISCUSSION

Photoreceptor light adaptation encompasses a complex set of molecular changes by which the cell adjusts to the ambient level of illumination. One manifestation of light adaptation is an extension of the range of intensities over which the cell is able to operate (Torre et al., 1995) beyond the restricted range that would apply as a result of the exponential saturation that occurs in the absence of adaptational changes (Matthews et al., 1988). A second manifestation is the gentle decline in flash sensitivity, according to Weber's Law, which is typically observed over the cell's operating range (Fig. 6 B). Our aim has been to account for these phenomena through a molecular model that we can express in quantitative terms, and for which most of the parameters can be measured. The primary new interpretations of our work are that light adaptation is characterized by the following: (1) an invariant gain of the amplifying steps; (2) a large reduction in the time constant of cGMP hydrolysis, which provides the dominant factor in desensitization of the biochemical cascade; and (3) a smaller reduction in the lifetime of activated rhodopsin. In addition, it is well known that guanylyl cyclase is activated, and that the $K_{1/2}$ of the cGMP-gated channels is reduced. Here, we emphasize that these two calcium-dependent phenomena act to sensitize (rather than desensitize) the response, by preserving an appropriate working level of circulating current.

Koutalos et al. (1995a,b) undertook a similar examination of range extension and sensitivity adjustment in salamander rods during light adaptation. They identified, and quantified, the roles of three calcium-dependent molecular processes: (1) the activation of guanylyl cyclase; (2) the "down regulation of PDE activity," which they identified as including recoverin-dependent and non-recoverin–dependent components; and (c) modulation of the $K_{1/2}$ for cGMP-gating of the channels. We shall compare their results and interpretations with ours as we proceed.

Light Adaptation Does Not Alter the Gain of the Amplifying Steps of Phototransduction

Our results strongly support the conclusion that there is no change in the gain of any of the amplifying steps in phototransduction at the intensities and durations of light adaptation used in our experiments. The theoretical basis for this assertion comes from the analysis un-

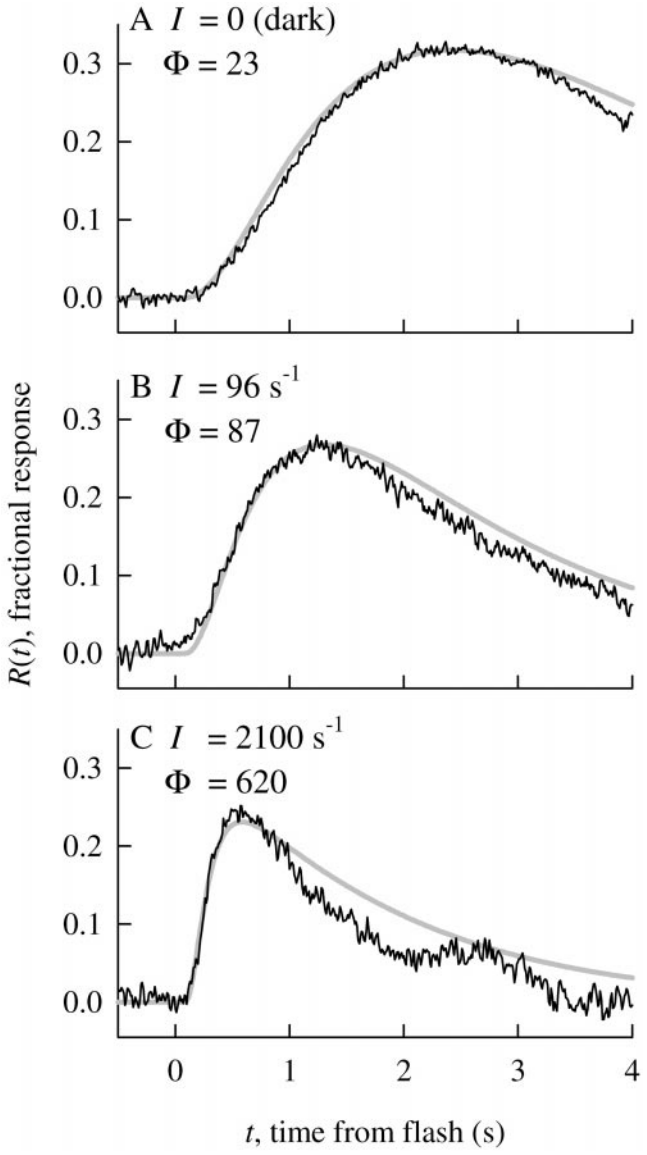

FIGURE 13. "Calcium-clamped" dim-flash responses, reproduced from the data of Figure 10 of Fain et al. (1989), compared with the predictions of our model. In the three panels, the backgrounds delivered: $I = 0$ (dark-adapted), 96, and 2,100 photoisomerizations per second, and the test flashes delivered $\Phi = 23$, 87, and 620 photoisomerizations (assuming a collecting area of 40 μm^2, for light polarized in the preferred orientation). In each case, the rod had been allowed to equilibrate to the adaptational state for several minutes. It was then exposed to "low-Ca^{2+}, 0-Na^+ solution" designed to minimize flash-induced changes in $Ca^{2+}{}_i$ (see Fain et al., 1989, for further details) and, after 5 s, a dim test flash was delivered; 9 s later, a bright flash was given, to measure the circulating current, and then the bathing solution was returned to Ringer's. The solution change with flash delivery was repeated at least four times for each panel. The theory traces have been simulated with the model in the APPENDICES, using the standard parameter values in Table IV, with the following exceptions: $A = 0.045\ s^{-2}$, $\tau_{R,Dark} = 0.4$ s, $\tau_E = 1.5$ s, and $\beta_{Dark} = 0.8\ s^{-1}$. In addition, the following parameter values were specific to the three panels: $\beta(I) = 0.8$, 1.7, and 10.1 s^{-1}, and $\tau_R(I) = 0.95$, 0.27, and 0.13 s. These values are determined by application of the steady-state model, with the exception of the value $\tau_R = 0.95$ s used for the dark-adapted response ($I = 0$) in A. A possible rationale for this relatively high value is that $Ca^{2+}{}_i$ may have risen during the "clamping" exposure, reducing the free RK to ~0.44 of the level it would normally be in the dark in Ringer's. The traces in B and C have been corrected for slight baseline drifts, of 0.01 and 0.027 pA s^{-1}, respectively.

derlying Eq. 6, which shows that, if the fractional response is invariant at early times, then the initial time course of flash-activated PDE activity must be common. Hence, the empirical test is provided by experiments in which flash responses are scaled as the fractional change in cGMP-activated current. These experiments show that all the scaled responses to a flash of any given intensity initially follow a common trajectory, independent of background illumination (Figs. 3 and 12 E), and, more generally, that the scaled responses to all flashes begin rising along a single trajectory when they are further divided by the test flash intensity (Fig. 4). Thus, the results of Fig. 4 place on a solid foundation the suggestion made previously by Torre et al. (1986; Figure 5) and Fain et al. (1989; Figure 10) for just one or two background intensities. Therefore, our experiments show that, during light adaptation, the activation phase of transduction is unaltered at the level of the G-protein cascade, and that what changes is instead the time of onset of recovery. This conclusion is further supported by simulation of the equations that describe the entire cascade (see APPENDICES). These simulations accurately describe the observed responses over the first 250 ms, on the assumption that there is no change in the amplification constant A of phototransduction during light adaptation (Fig. 12, A–D).

Our conclusion that the amplification of phototransduction is unaltered by adaptation is at variance with conclusions drawn by several other investigators, who have reported that the early rising phase of the response is reduced by adaptation (Gray-Keller and Detwiler, 1994; Jones, 1995) or by lowered Ca^{2+} concentration (Lagnado and Baylor, 1994). We think that a major factor contributing to these previous interpretations has been a lack of appreciation of the magnitude of the reduction that occurs in the inactivation time constants, on backgrounds of moderate to high intensity. Thus, on a background that halves the circulating current of a salamander rod, we predict that two of the inactivation time constants, τ_R and $1/\beta(I)$, will each have declined to ~150 ms, so that deviations from a common early rise will be expected to occur by ~100 ms. Hence, the observation of a lowered slope of the rising phase at times later than this does not indicate a reduced amplification constant.

An additional factor that may explain the apparent difference between our interpretations and those of Lagnado and Baylor (1994) is that their reported $K_{1/2}$

for the Ca dependence of the effect was 35 nM, whereas we think it likely that, in our experiments, the steady Ca^{2+} concentration remained much higher than this level. For our brightest backgrounds, of 2,000–3,000 photoisomerizations per second, the steady circulating current was reduced to roughly 20% of its dark-adapted level, so that the steady Ca^{2+} concentration ought to have been reduced to a comparable fraction, i.e., to ~120 nM. At such a concentration, the mechanism they describe would be expected to reduce the gain by only a small amount (<10%).

Elevated Phosphodiesterase Activity Evoked by Steady Light

We have made new measurements, and provided further understanding, of the light-evoked increase in steady PDE activity, which we have quantified through the steady-state rate constant $\beta(I)$ of cGMP hydrolysis. First, we have been able to estimate $\beta(I)$ at higher intensities than previously (up to 2,600 photoisomerizations per second) by comparing the predictions of our mathematical model with the results of experiments performed using the IBMX-jump method of Hodgkin and Nunn (1988) (Fig. 8). Use of this theoretical approach provides estimates of $\beta(I)$ that we think should be more accurate than those obtained using the conventional derivative method; that method yields underestimates of $\beta(I)$, as a result of the rapid decrease in guanylyl cyclase activity, α, elicited by the massive rise in cytoplasmic Ca^{2+} concentration that inevitably accompanies the IBMX-induced opening of cGMP-gated channels. Second, we have provided (in Eq. B7) a formulation for the dependence of $\beta(I)$ on fundamental parameters of the cascade, as

$$\beta(I) = \beta_{\mathrm{Dark}} + \frac{A\tau_{\mathrm{R}}(I)\tau_{\mathrm{E}}}{n_{\mathrm{cG}}} I, \qquad (11)$$

where $\tau_{\mathrm{R}}(I)$ is the effective lifetime of R* in the presence of the background, τ_{E} is the effective lifetime of G*-E*, A is the amplification constant of transduction, n_{cG} is the Hill coefficient of channel activation, and I is the intensity of steady light. Third, we have shown that this relatively simple expression provides a good account of the experimentally measured dependence of $\beta(I)$ on steady light (Fig. 9). Fourth, we have shown that the dark-adapted rate constant of cGMP hydrolysis (β_{Dark}) appears to exhibit greater variability from cell to cell than does the light-stimulated increase in $\beta(I)$. Therefore, we suggest that β_{Dark} is determined by factors other than, or additional to, the four that scale the intensity in Eq. 11. Fifth, we have extended the analysis of Nikonov et al. (1998), which showed that in darkness $1/\beta_{\mathrm{Dark}}$ acts as one of the time constants of recovery in the transduction cascade, to the general case, by showing that $1/\beta(I)$ plays the same role during light adaptation (Fig. 12). Finally, we have established that, of the three main time constants in the cascade, $1/\beta$ is the one that undergoes the greatest change during light adaptation (Fig. 11).

Our Eq. 11 above is closely analogous to the expression for PDE activation used by Koutalos et al. (1995b) in their Equations 2 and 4. The difference is that their formulation used the single calcium-dependent parameter $\beta^*(Ca)$ to express the light dependence of PDE activity, whereas we use the composite term $A\tau_{\mathrm{R}}(I)\tau_{\mathrm{E}} / n_{\mathrm{cG}}$, which comprises four parameters, each of which has a defined physical meaning and can be estimated independently. Since we have provided evidence that A is constant and that τ_{E} is, at most, weakly dependent on adaptation, and since we have no reason to suspect a change in n_{cG}, the calcium dependence of β^* expressed in their (Koutalos et al., 1995b) Equation 2 should correspond to the calcium dependence of τ_{R} in our formulation; this is specified in Eq. A12 and APPENDIX C.

Inspection of Fig. 9 shows that there is an approximately fourfold difference between our description and that of Koutalos et al. (1995b) for the predicted dependence of $\beta(I)$ on I. Thus, at a background of 1,000 photoisomerizations per second (~50 photons μm^{-2} s^{-1}), the Koutalos et al. (1995b) description gives $\beta(I) \approx 2.5$ s^{-1}, whereas our description gives $\beta(I) \approx 10$ s^{-1}. In addition, there is a smaller discrepancy in the dark-adapted value in the two cases: Koutalos et al. (1995b) reported $\beta_{\mathrm{Dark}} \approx 0.3$ s^{-1}, whereas our experiments gave 0.8–1.6 s^{-1}. These differences are illustrated by the lower curves in Fig. 9: the dotted traces plot the predictions of Equation 2 from Koutalos et al. (1995b), who considered two possible levels of dark calcium concentration. These curves significantly underestimate the measurements of $\beta(I)$ versus I made not only in our study, but also by Hodgkin and Nunn (1988) and Cornwall and Fain (1994).

Contribution of Individual Molecular Mechanisms to Overall Adaptational Behavior

The effect of increasing background intensity is to increase the steady rate constant of cGMP hydrolysis, $\beta(I)$, thereby lowering the cGMP concentration, and driving the photoreceptor towards saturation. In our view, the primary function of "adaptation" is to prevent the rod from being driven into saturation, thereby preventing the massive reduction in sensitivity that would otherwise occur. Three molecular mechanisms are known to help the rod evade saturation, and each is calcium-dependent: (1) the GCAP-dependent activation of guanylyl cyclase ("GCAP mechanism"); (2) the recoverin-dependent increase in rhodopsin kinase activity ("Rec mechanism"); and (3) the calmodulin-dependent decrease in the $K_{1/2}$ of the cGMP-activated channels ("CaM mechanism").

In an attempt to evaluate the relative importance of these mechanisms in the maintenance of circulating current and sensitivity, we provide in Fig. 14 a series of

calculations for the model rod in which the three mechanisms are either present or absent in all combinations. In considering the following analysis, it is important to bear in mind that we are not performing direct experimental manipulations, but that we are instead investigating the performance of our model when we manipulate it in ways designed to simulate alterations in the presumed molecular mechanisms. Nevertheless, we think that important lessons can be learned.

A, B, and C (Fig. 14) present the predictions for steady-state current, sensitivity, and fractional sensitivity, respectively, in the format of Fig. 6, with the following color coding. In each case, blue denotes the CaM mechanism alone; green denotes the Rec mechanism alone; and red denotes the GCAP mechanism alone. The other three colors denote paired combinations of these mechanisms: CaM + Rec (cyan); CaM + GCAP (magenta); and Rec + GCAP (yellow). Black denotes the case with none of the mechanisms enabled, whereas dark gray denotes the normal case with all three mechanisms active. In accordance with the conclusions of Koutalos et al. (1995b), and as we discuss below, the curves in Fig. 14 (A and B) are consistent with the idea that the most potent of the calcium-dependent adaptational mechanisms is the activation of GC, and that the least potent is the CaM-dependent shift in K_{cG} of the channels.

In Fig. 14 A, an additional ordinate scale is provided for $Ca(I)$, since the steady-state calcium concentration is uniquely determined by the steady circulating current. At any fixed level of calcium, one can think of the rightward shift of each curve relative to the leftmost curve as the predicted effect of that mechanism (or combination of mechanisms) in extending the intensity range over which the cell can operate at that particular calcium level.

Contributions to Absolute Sensitivity and Fractional Sensitivity

Since light adaptation leads to reduced flash sensitivity, one might naively hope to determine the contribution of the individual molecular mechanisms to the overall desensitization that is observed, but such a division is fraught with difficulty. The problem arises because the feedback loop underlying photoreceptor light adaptation leads to the prevention of sensitivity loss, rather than to desensitization per se. Hence, as illustrated in Fig. 14, the role of each of the calcium-modulated feedback mechanisms is to sensitize rather than desensitize the cell. To appreciate this, one needs to consider a vertical line drawn on Fig. 14B at any arbitrary intensity: the vertical spacing between the traces then gives the predicted effect of that mechanism (or those mechanisms) on sensitivity at the particular background level.

For example, imagine a steady background of 1,000 photoisomerizations per second in Fig. 14 B, and consider the predicted effect of separately disabling the three individual mechanisms. With all mechanisms functional, the relative sensitivity of the model rod is calculated as 0.032 (gray trace); with the CaM mechanism disabled, it should be indistinguishable from this, at 0.032 (yellow trace); with the Rec mechanism disabled, it should be down to 0.0136 (magenta trace); and with the GCAP mechanism disabled, it should be greatly depressed, to 0.0031 (cyan trace). Hence, the model predicts that, at this intensity, the CaM mechanism has negligible effect on sensitivity, whereas the Rec and GCAP mechanisms sensitize the rod by factors of 2.3-fold and 10-fold, respectively (in each case with respect to the situation where the mechanism is disabled).

In a similar manner, one can assess the predicted contributions of the different mechanisms to the fractional sensitivity plotted in Fig. 14 C. In comparing B and C in Fig. 14, perhaps the most prominent feature is the tight grouping of the traces in C compared with the wide spacing in B. For a line drawn at 1,000 photoisomerizations per second in Fig. 14 C, the solid curves are separated vertically by a factor of <2. This tight grouping means that our model predicts the "biochemical sensitivity" of the cascade at this fixed intensity to be barely affected by the presence or absence of the different molecular mechanisms. How might mechanistic insensitivity of this type come about?

Desensitization of the Biochemical Cascade: Kinetic Roles of $\beta(I)$ and $\tau_R(I)$

The decline in fractional sensitivity in Fig. 14 C must be caused by changes in the kinetics of inactivation of the biochemical response, i.e., by the shortening of the time constants of the signal integrating steps of the cascade (with possible contributions by dynamic feedback through the flash-induced change in $Ca^{2+}{}_i$). That this is so, may be seen from the fact that the rising phase of the fractional response $R(t)$, and hence of $\Delta cG(t)/cG(I)$, is unaffected by the presence of background illumination (Figs. 3, 4, and 12). Hence, the decline in S, which is measured at the peak of the response, occurs because the time to peak becomes shorter. In the same way, the theoretical traces in Fig. 14 C reflect the reductions in biochemical sensitivity predicted to result from accelerated recovery kinetics, whereas the traces in Fig. 14 A reflect the time-invariant reductions in sensitivity predicted to result from response compression, and the two sets of traces multiply together to yield the overall reductions in sensitivity predicted in Fig. 14 B.

Our simulations further support the conclusion that dynamic calcium feedback contributes little to the decline in relative fractional sensitivity. Thus, the dotted curve in Fig. 14 C computed for a rod with $Ca^{2+}{}_i$ clamped (to the level set by a background presented in Ringer's) lies very close to the gray curve obtained for a

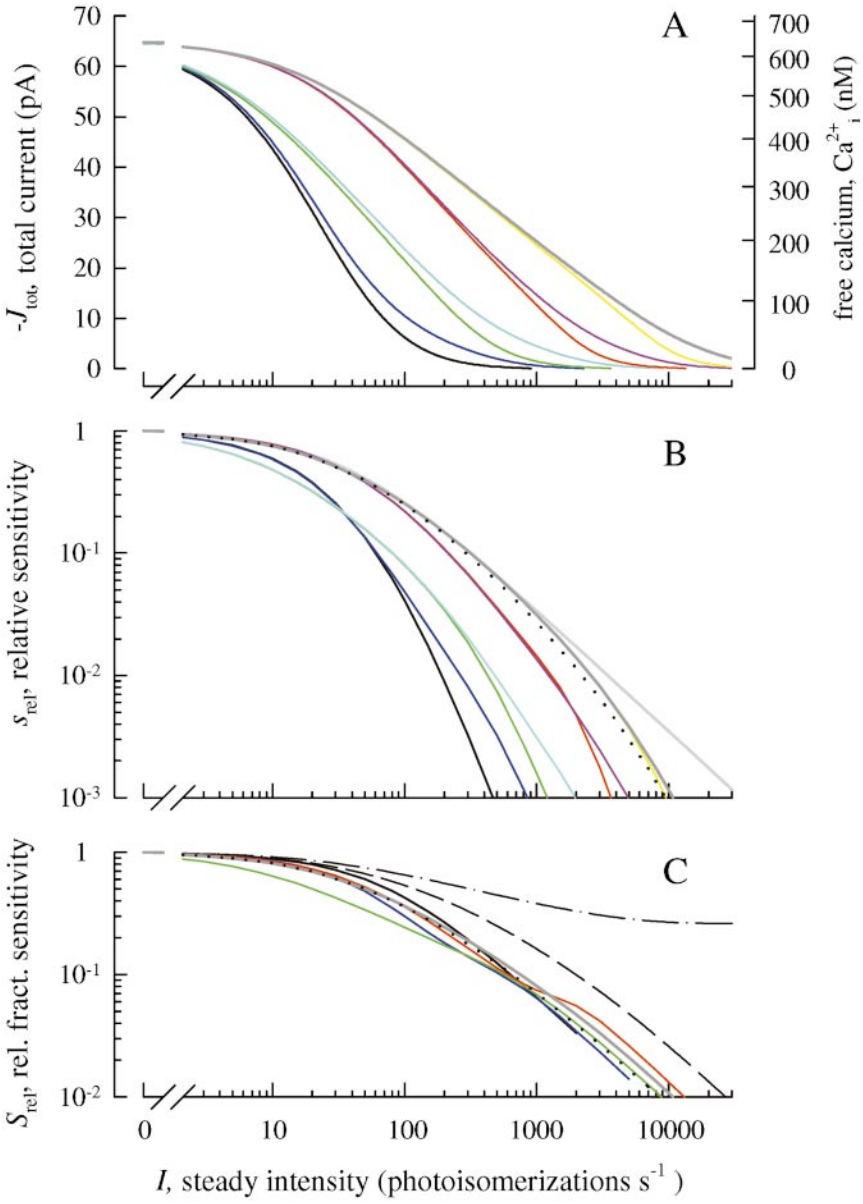

FIGURE 14. Analysis of the contributions of different molecular mechanisms to light adaptation. All traces (except the dashed traces in C) were computed with the model salamander rod presented in the APPENDIX. The color coding identifies the eight combinations of the three calcium-dependent feedback mechanisms. (Blue) The calmodulin-dependent shift in K_{cG} of the cGMP-activated channels ("CaM mechanism") alone. (Green) The recoverin-dependent inactivation of rhodopsin kinase ("Rec mechanism") alone. (Red) The GCAP-dependent activation of guanylyl cyclase ("GCAP mechanism") alone. (Black) All mechanisms inactivated. (Cyan) CaM + Rec mechanisms; (magenta) CaM + GCAP mechanisms; and (yellow) Rec + GCAP mechanisms. Dark gray (rather than white): all mechanisms active. (Light gray) Weber's Law, $S_{rel} = I_0/(I+I_0)$, with $I_0 = 40$ photoisomerizations per second. (A) Steady circulating current, $j(I)$; this is as in Fig. 6 A, except that the scale is in absolute units of pA. (B) Relative sensitivity, $s_{rel} = s(I)/s_{Dark}$. The dotted curve shows the prediction of the model for the experimental condition illustrated in Fig. 13, in which Ca^{2+}_i is clamped to the level set by the steady background to which the rod is exposed in Ringer's. (C) Relative fractional sensitivity, $S_{rel} = s_{rel}/J_{rel}$. To avoid crowding, the traces for pairs of mechanisms (cyan, magenta, and yellow) have not been shown. Two additional curves are shown dashed, that were computed using a three time constant (τ_R, τ_E, and $1/\beta$) model of calcium-clamped rods (Equation 19 of Nikonov et al., 1998). (Dashed trace) β was varied according to the full model, while τ_R was held at its dark level. (Dot-dash trace) β was held at its dark level, while τ_R was varied according to the full model.

rod operating normally in Ringer's, with Ca^{2+}_i free to change dynamically. Thus, we are led to the conclusion that the primary factors contributing to the decline in fractional sensitivity are the declines in the two time constants, τ_R and $1/\beta(I)$ (Figs. 11 and 13). The tight "bunching" in Fig. 14 C indicates that, in the presence of the normal drop in steady-state Ca^{2+}_i, the combined effect of the reductions in these two time constants in the model rod is computed to be roughly the same, irrespective of the combination of mechanisms enabled. Thus, in a case where a greater reduction in τ_R occurs, there is a smaller increase in β, and, hence, a smaller reduction in $1/\beta$, so that the resulting time course is quite similar.

A slight exception to this trend occurs for the green trace (Rec mechanism alone), which differs significantly from the other traces at relatively dim backgrounds. This occurs because, when both the other feedback mechanisms are disabled in our model, the Rec mechanism is brought into play at relatively low intensities, and the shortening of R* lifetime causes a more pronounced reduction in biochemical sensitivity than occurs in the full model.

Relative Importance of $\beta(I)$ and $\tau_R(I)$ in the Normal Case

To assess the relative importance of the increased PDE rate constant of cGMP hydrolysis (β) and the Rec-mediated shortening of R* lifetime (τ_R) in mediating the observed reduction in fractional sensitivity in the normal case, we now consider the effect of the altered time constants in a cascaded chain of integrating stages. Thus, we consider the dim-flash approximation derived by Nikonov et al. (1998; see their Equation 19) under calcium-clamped conditions that comprises a cascade of three time constants: $\tau_R(I)$, τ_E, and $1/\beta(I)$.

The two dashed traces in Fig. 14 C investigate the predicted contributions to the normal case of changes in $1/\beta$ alone and in τ_R alone. For these two traces, one of the time constants has been held at its dark-adapted level, while the other has been varied according to the predictions of the full model. Clearly, neither of these situations can occur in reality, and we present them purely in the context of attempting to separate the contributions of the two time constants to the normal behavior. These traces show that the contribution of $1/\beta(I)$ (dashed) is predicted to significantly outweigh that of $\tau_R(I)$ (dot-dashed), especially at higher background intensities where the decrease in R* time constant saturates.

We reiterate the proviso stated earlier, that the interpretations we have reached above have been obtained from analysis of the predictions of our model, rather than from direct experimental manipulation.

Bathtub Analogy of Reactions Governing cGMP Concentration

In an attempt to provide a more intuitive understanding of the role of the increased rate constant of cGMP hydrolysis in desensitizing the fractional response and accelerating the recovery, we now present an informal description, which we call the "bathtub analogy" of the reactions governing cGMP.

Imagine a bathtub, in which the depth of water represents the cGMP concentration. The rate at which water runs into the tub from a tap represents the activity of guanylyl cyclase (α), and the rate at which water drains out of the tub is proportional both to the depth of the water and also to the size of the drain, which represents the PDE activity, β. When a steady state is reached, the depth of water will equal the rate of influx divided by the rate constant of efflux; i.e., $cG(I) = \alpha(I)/\beta(I)$. Now imagine that the size of the drain is briefly enlarged, before returning to its previous size, causing a transient increment in the rate of efflux, $\Delta\beta(t)$. This will elicit a transient drop in water level, $\Delta cG(t)$, followed by eventual recovery to the original steady level. The question is: with what time course does the water level recover, once the drain has returned to its original size? The answer is that it recovers exponentially, according to a rate constant $\beta(I)$, or time constant $1/\beta(I)$.

Next, imagine that the size of the drain is permanently enlarged, thus increasing $\beta(I)$ and, in addition, that the tap is correspondingly opened up to increase the steady influx of water, thus increasing $\alpha(I)$. If the two parameters are increased in the same ratio then the steady-state depth of water, $cG(I)$, will remain unchanged. Suppose now that the same incremental stimulus is given as previously—a transient additional opening of the drain, $\Delta\beta(t)$. If this stimulus is delivered instantaneously, it will cause the same initial drop in water level as previously. But, very importantly, the recovery will occur more rapidly. Thus, the water level will begin rising more rapidly than previously, because the influx of water through the tap is faster, yet it will reach the same steady level as before; therefore, it must reach that level sooner.

In general terms, the effect of enlarging the drain will be to accelerate the rate at which the water level re-equilibrates whenever it is perturbed, whereas the effect of a steady opening-up of the tap will simply be to scale-up the depth of water in the tub. Importantly, if one expresses the depth during the response as a fraction of its level before the stimulus, (i.e., as $cG(t)/cG(I)$), then the response will be independent of the rate of influx through the tap, provided that the rate is constant; i.e., that $\alpha(t) = \alpha(I)$.

Flux of cGMP

The existence of the powerful Ca^{2+}-mediated feedback loop results in relatively small changes in concentration of cGMP and Ca^{2+} during light adaptation, but quite large changes in the flux of cGMP, corresponding to large increases in α and β. The flux of cGMP in the model rod increases from 3.5 $\mu M\ s^{-1}$ in darkness to $\sim$27 $\mu M\ s^{-1}$ in the presence of a background producing I = 3,000 photoisomerizations per second, whereas β increases from 1.0 to 21 s^{-1}, and cG only declines from 3.5 to 1.1 μM. Experimental measurements with the ^{18}O method (applied to toad rods in the intact retina) have yielded even larger changes in the flux of cGMP (Dawis et al., 1988): from $\sim$2 $\mu M\ s^{-1}$ in darkness to $\sim$100 $\mu M\ s^{-1}$ during exposure to a steady light of I = 3,000 photoisomerization per second.

Some years ago, it was proposed that the light-induced changes in cGMP flux, per se, might underlie the photoreceptor's electrical response (Goldberg et al., 1993; Dawis et al., 1988). Although that proposition is no longer tenable, in the face of overwhelming evidence that the change in concentration of cGMP is the signal that determines the electrical response, it remains conceivable that the flux of cGMP might play some role in adaptation of the photoreceptor. Certainly, the flux constitutes a significant metabolic load: in the presence of a background producing 3,000 photoisomerizations per second the calculated cGMP flux

of ~27 μM s^{-1} requires an equal rate of GTP utilization by guanylyl cyclase, and ultimately of ATP utilization. For comparison, maintenance of the 16 pA circulating current at the same intensity requires ATP utilization at a rate of ~50 μM s^{-1}.

Relative Robustness of Conclusions

The reader may rightfully inquire as to the relative certainty (or robustness) of our conclusions, in particular, of those involving calculations with the model rod presented in the APPENDICES. We think that our conclusions fall into the following several categories of certainty: (a) robust, conclusions obtained through analysis of the experimental results with the "activation-only" form of the model; (b) reasonably robust, conclusions obtained by analysis using the full model under conditions of fixed Ca^{2+} concentration; and (c) less robust, conclusions dependent on the full model when the Ca^{2+} concentration is changing dynamically.

Thus, at the highest level of certainty is our conclusion that the amplification constant of phototransduction is unaltered by adaptation, since this was obtained by analysis of experimental traces simply scaled according to the steady circulating current (Figs. 3, 4, and 9). Next in degree of robustness, we consider to be the calculated dependence of β on I (Figs. 8 and 9), because this depends primarily on the Hill relation for channel activation, in conjunction with steady synthesis and hydrolysis of cGMP. Although our correction of the estimates at high background intensities, by analysis with the model rod, introduces some model dependence into the estimated values of β, this has little effect on the overall shape of the relation (Fig. 9).

We also consider the characterization of the step/flash effect as a calcium-dependent shortening of a "nondominant time constant" (Figs. 10 and 11) to be a robust conclusion, especially in light of our evidence that the amplification constant is not affected by adaptation. However, our identification of this nondominant time constant as the effective lifetime of R* (and specifically our description of this lifetime as being determined by the calcium-dependent inhibition of rhodopsin kinase by recoverin) clearly depends on our model and on the values adopted for the parameters of the recoverin binding reactions (APPENDIX C). Although these values have been taken from the biochemical literature, they have not been obtained for salamander rod proteins, and there are substantial differences in the estimates from different laboratories and for different species.

Next in robustness are our conclusions concerning the contributions of the different calcium-dependent mechanisms to the cell's operating range, i.e., its response versus intensity relation (Fig. 14 A). Although we feel confident that the relative contributions predicted for the three mechanisms are broadly correct, we acknowledge that the model utilizes a number of calcium-dependent parameters whose exact values remain somewhat uncertain.

Finally, we consider our predictions of response kinetics, and of parameters derived from the response kinetics, to be the least robust aspects of our conclusions, since the underlying calculations involve dynamic changes in $Ca^{2+}{}_i$ and, therefore, dynamic changes in all Ca-dependent processes in the rod. Accordingly, the predicted form of sensitivity as a function of background intensity (Fig. 6, B and C, and Fig. 14, B and C) cannot be considered as particularly robust; i.e., the shape of the relation is likely to be model-dependent. Despite this qualification, we think our conclusion that the increase in $\beta(I)$ represents the dominant factor in desensitizing the rod's biochemical cascade remains robust, since the effect is present in calcium-clamped rods (Fig. 13).

Limitations of Our Present Description of Transduction

Our present model of the salamander rod achieves a good description of the steady-state dependence of circulating current (Fig. 6 A) and sensitivity (Fig. 6, B and C) on background intensity, and a good description of the kinetics of responses obtained under constant calcium conditions (Figs. 12 and 13). Where it falls down is in its prediction of the exact form of the response kinetics under conditions where $Ca^{2+}{}_i$ is free to change; i.e., in normal Ringer's solution (traces not shown). Thus, the numerical solutions do not yet provide a satisfactory description of the overall family of flash responses in Ringer's, or even of just the dim-flash response when tested over the full range of adapting intensities. We emphasize that what we seek is a model with a single set of parameters that are consistent with all relevant measurements in the literature, including measurements of $Ca^{2+}{}_i$, the concentrations and binding parameters of the calcium binding proteins, etc. We think that the key features remaining to be resolved relate to the dynamics of shut-off of the various proteins, and entwined with these issues are kinetic aspects of the calcium buffering provided by the various calcium binding proteins, including recoverin, guanylyl cyclase activating proteins, and calmodulin.

We do not underestimate the problems that remain in obtaining a complete molecular description of the rod's response to flashes on backgrounds. But at this stage, we are confident, first, that the conventional description of activation is accurate and, second, that the main factors underlying light adaptation have been described adequately in steady-state terms. However, we think that further information will be needed about dynamic changes in these inactivation steps, before a definitive molecular description of the rod's electrical response can be provided.

TABLE III

Definitions of Variables in the Equations

Symbol	Units	Value‡	Definition	Defined in Eq.
Primary variables				
I	isomerizations s^{-1}	0	Light intensity	
Φ	isomerizations	0	Intensity of brief flash	
R^*	molecules	0	Activated rhodopsin molecules per outer segment	A1
E^*	subunits	0	Activated PDE subunits per outer segment	A2
cG	μM	3	Cytoplasmic free concentration of cGMP	A3
Ca	nM	640	Cytoplasmic free concentration of Ca^{2+}	A4
β	s^{-1}	1	Rate constant of cGMP hydrolysis over outer segment	A5
j_{cG}	pA	−60	Current carried by cGMP-activated channels	A6
j_{ex}	pA	−5	Electrogenic current carried by exchanger	A9
j_{tot}	pA	−65	Total circulating current	A14
Variables with explicit Ca^{2+} dependence				
α	μM s^{-1}	3.6	Rate of synthesis of cGMP by guanylyl cyclase	A10
K_{cG}	μM	32	cGMP concentration for half-maximal channel opening	A11
τ_R	s	0.35	Time constant of R* inactivation	A12
Rec	μM	18	Free concentration of recoverin in outer segment	C3
RK	μM	1.7	Free concentration of RK in outer segment	C1
$B_{Ca,\,Rec}$		44	Ca^{2+}-buffering power due to recoverin	C5

‡Value in dark.

APPENDIX A: THE EQUATIONS OF PHOTOTRANSDUCTION

We, and other groups, have previously presented equations describing the G-protein cascade of phototransduction that embody insights and formalisms from numerous biochemical and physiological investigations. In this Appendix we summarize those equations, and we acknowledge their first use (even when in slightly different form) using the following abbreviations: FKL (Fesenko et al., 1985), KM (Kawamura and Murakami, 1986), HN (Hodgkin and Nunn, 1988), FMRT (Forti et al., 1989), LCM (Lagnado et al., 1992), LP (Lamb and Pugh, 1992), and NEP (Nikonov et al., 1998).

In general, each of the variables is a function both of the steady background intensity (I) and the time (t) after a flash, e.g., $j(I, t)$, but for simplicity, we will usually drop one or both of these independent variables. Thus, we will usually denote the time-dependent form as $j(t)$, or often simply as j where this is unambiguous, whereas we will denote its steady state value $j(I,\infty)$ simply as $j(I)$, with its dark-adapted steady value denoted as j_{Dark}. Although many of the variables are calcium-dependent, in general, this will not be denoted explicitly. For brevity, the definitions of all the variables and constants are given in Tables III and IV, respectively.

Differential Equations

The rates of supply and removal of the active species R^*, E^*, cG, and Ca can be expressed in terms of the four differential equations.

Activated rhodopsin:

$$\frac{dR^*}{dt} = I - k_R R^*. \tag{A1}$$

Activated PDE:

$$\frac{dE^*}{dt} = \nu_{RE} R^* - k_E E^*. \tag{A2}$$

Free cGMP concentration [KM (4)]:

$$\frac{dcG}{dt} = \alpha - \beta cG. \tag{A3}$$

Free Ca^{2+} concentration [NEP (12)]:

$$\frac{dCa}{dt} = -\frac{(1/2) f_{Ca} j_{cG} - j_{ex}}{\Im V_{cyto} B_{Ca}}. \tag{A4}$$

In each case, the first term on the right represents generation, whereas the second term represents removal. In the first three equations, the rate constants of turnover of the active substance are the following: k_R ($= 1/\tau_R$) for R^*, k_E ($= 1/\tau_E$) for E^*, and β for cG. As a simplification in writing Eq. A2, any depletion in the pools of activatable G-protein and PDE, which may occur with intense flashes, has been ignored. In addition, a short delay t_{eff} contributed cumulatively by several of the activation steps has also been ignored, but can readily be accounted for by a simple time shift.

Equations Relevant to the Rising Phase

Two variables describing the rising phase, which do not depend explicitly on Ca^{2+} concentration, are specified by the following equations.

TABLE IV

Definitions and Standard Values of Constants in the Equations

Symbol	Units	Value	Definition	Equation
Activation of PDE and hydrolysis of cGMP				
A	s^{-2}	0.08	Amplification constant of transduction	A7
ν_{RE}	s^{-1}	220	Rate of E* formation per fully activated R*	A2
V_{cyto}	pl	1	Cytoplasmic volume of the outer segment	A4, A8
B_{cG}		2	Buffering power of the cytoplasm for cGMP	A8
β_{sub}	s^{-1}	1.8×10^{-4}	Rate constant of cGMP hydrolysis per E* subunit	A5, A8
k_{cat} / K_m	$s^{-1}\ \mu M^{-1}$	440	Hydrolytic efficacy of fully-activated PDE dimer	A8
N_{Av}	mol^{-1}	6×10^{23}	Avogadro's number	A8
$\Im$	C mol^{-1}	96,500	Faraday	A4
Circulating electrical current				
$j_{cG,\,max}$	pA	−7,000	Maximal cGMP-activated current per outer segment	A6
n_{cG}		2	Hill coefficient of cGMP channel activation	A6
t_{eff}	ms	10	Overall delay contributed by short steps	
τ_m	ms	20	Membrane capacitive time constant	
Rate constants of inactivation				
$k_{R,\,max}$	s^{-1}	12	Rate constant of R* inactivation when all RK is free	A12
τ_E	s	1.6	Time constant of inactivation of G*–E* complex	A2
β_{Dark}	s^{-1}	1.0	Rate constant of cGMP hydrolysis in darkness	A5
Calcium influx and efflux				
f_{Ca}		0.17	Fraction of cGMP-activated current carried by Ca^{2+}	A4
K_{ex}	nM	1,500	Ca^{2+}concentration for half-maximal exchange current	A9
$j_{ex,\,sat}$	pA	−17	Saturated exchange current at high Ca^{2+}concentration	A9
Guanylyl cyclase activation				
K_{cyc}	nM	150	Ca^{2+}concentration for half-maximal cyclase activity	A10
n_{cyc}		2	Hill coefficient for cyclase activation by Ca^{2+}	A10
α_{max}	$\mu M\ s^{-1}$	50	Maximum value of α at low Ca^{2+}concentration	A10
$\frac{\alpha_{min}}{\alpha_{max}}$		0.02	Suppression ratio of α from high to low Ca^{2+}concentration	A10
Recoverin effect on rhodopsin kinase				
K_1	μM	4.5	K_1^2 is dissociation constant for Rec + $2Ca^{2+}$	C2, C4
K_2	μM	230	Dissociation constant for Rec · $2Ca^{2+}$ + Membrane	C2, C4
K_4 (= K_3)	μM	3.4	Dissociation constant for Rec · $2Ca^{2+}$ · M + RK	C2
M	μM	6,000	Membrane concentration in terms of which K_2 is expressed	C2
Rec_{tot}	μM	34	Total concentration of recoverin in outer segment	C1–C3
RK_{tot}	μM	7	Total concentration of RK in outer segment	
Calmodulin effect on channel activation				
K_{CaM}	nM	60	Ca^{2+}concentration for half-maximal calmodulin effect	A10
n_{CaM}		2	Hill coefficient for calmodulin activation by Ca^{2+}	A10
$K_{cG,\,min}$	μM	13	Minimum value of K_{cG} at low Ca^{2+}concentration	A10
$K_{cG,\,max}$	μM	32	Maximum value of K_{cG} at high Ca^{2+}concentration	A10

Rate constant of cGMP hydrolysis [LP (4.3)]:

$$\beta = \beta_{Dark} + \beta_{sub} E^*. \tag{A5}$$

cGMP-activated channel current [FKL]:

$$j_{cG} = j_{cG,max} \frac{cG^{n_{cG}}}{cG^{n_{cG}} + K_{cG}{}^{n_{cG}}}. \tag{A6}$$

Nevertheless, it should, be borne in mind that K_{cG} in Eq. A6 is a function of *Ca*; see Eq. A11.

From the equations above, it is possible to solve for the rising phase of the rod's response to illumination, and the solution is characterized by an amplification constant defined as follows:

Amplification constant [LP (6.9)]:

$$A = \nu_{RE} \beta_{sub} n_{cG}. \tag{A7}$$

where

Rate constant of cGMP hydrolysis per E* [LP (4.4)]:

$$\beta_{sub} = \frac{(1/2) k_{cat} / K_m}{V_{cyto} N_{Av} B_{cG}}. \tag{A8}$$

Equations Related to Recovery and Adaptation

The remaining equations relate primarily to the recovery phase and to adaptation, and the parameters are explicitly dependent on Ca^{2+} concentration. Two of these parameters, describing the electrogenic exchange current and the guanylyl cyclase activity, are well established in the literature.

Exchange current [LCM (1)]:

$$j_{ex} = j_{ex,sat}\frac{Ca}{Ca + K_{ex}}. \quad (A9)$$

Guanylyl cyclase [FMRT (16)]:

$$\alpha = \alpha_{min} + \frac{\alpha_{max} - \alpha_{min}}{1 + (Ca/K_{cyc})^{n_{cyc}}}. \quad (A10)$$

In addition, we present three new equations, the first being for the Ca^{2+}/calmodulin modulation of channel activation, and the next two characterizing the Ca^{2+}/recoverin/RK system. Whereas Koutalos et al. (1995b) formulated the calmodulin effect as a change in the scaling of current (their Equation 3), we have instead specified the effect as a shift in channel activation, according to:

Channel activation constant,

$$K_{cG} = K_{cG,max} + \frac{K_{cG,min} - K_{cG,max}}{1 + (Ca/K_{CaM})^{n_{CaM}}}. \quad (A11)$$

In Appendix C, we analyze the recoverin/RK system, and we develop equations specifying the free concentration of recoverin and of RK, and recoverin's Ca^{2+}-buffering power, in terms of the Ca^{2+} concentration. Here, we simply take the resulting variables, RK (from Eq. C1 with C3) and $B_{Ca,\ Rec}$ (from Eq. C5), and use these to specify the rate constant of R* decay, and the total Ca^{2+}-buffering power of the cytoplasm.

Rate constant of R* decay:

$$k_R = k_{R,max}\frac{RK}{RK_{tot}}. \quad (A12)$$

Ca^{2+}-buffering power:

$$B_{Ca} = 1 + B_{Ca,Rec} + B_{Ca,other}. \quad (A13)$$

Finally, the total circulating current of the outer segment is the sum of the current through the cGMP-activated channels and the electrogenic exchange current:

Total outer segment current:

$$j_{tot} = j_{cG} + j_{ex}. \quad (A14)$$

except that, when the membrane capacitive time constant (τ_m) is taken into account, a filtered version of this equation must be used.

Exposure to IBMX

To deal with exposure of the outer segment to IBMX, we assume that the PDE rate constant of cGMP hydrolysis (β) that occurs in Eq. A3 and is defined in Eq. A5, is inhibited (divided) by the following factor.

PDE inhibition factor:

$$1 + \frac{IBMX}{K_I}(1 - \exp(-t/\tau_I)), \quad (A15)$$

where $IBMX$ is the concentration of IBMX in the perfusate, t is time after the solution change, $\tau_I \approx 100$ ms is the time constant of equilibration, and $K_I = 10$ μM is the competitive inhibition constant.

APPENDIX B: THE STEADY STATE

The steady state of the system described in Appendix A may be determined by setting the derivatives in Eqs. A1–A4 equal to zero, and solving the resulting equations simultaneously with the other equations. Although it is not possible to obtain an analytical solution in terms of the steady background intensity (I), it is instead possible to adopt an inverse approach, because all the variables can be specified as functions of Ca^{2+}concentration. Hence, one may perform the following sequence of operations.

(a) Select a wide range of steady state values of $Ca(I)$.

(b) Calculate the steady-state Ca^{2+}-dependent variables: $j_{ex}(I)$, $\alpha(I)$, $K_{cG}(I)$, $RK(I)$, and $k_R(I)$.

(c) Substitute these values into Eqs. A1–A4 with the derivatives set to zero, and into Eqs. A5 and A6, to obtain respectively:

from Eq. A4,

$$j_{cG}(I) = 2j_{ex}(I)/f_{Ca}; \quad (B1)$$

from Eq. A6,

$$cG(I) = K_{cG}(I)(j_{cG,max}/j_{cG}(I) - 1)^{-\frac{1}{n_{cG}}}; \quad (B2)$$

from Eq. A3,

$$\beta(I) = \alpha(I)/cG(I); \quad (B3)$$

from Eq. A5,

$$E^*(I) = (\beta(I) - \beta_{Dark})/\beta_{sub}; \quad (B4)$$

from Eq. A2,

$$R^*(I) = k_E E^*(I)/\nu_{RE}; \quad (B5)$$

from Eq. A1,

$$I = k_R(I)R^*(I). \quad \text{(B6)}$$

By substitution of the definition of the amplification constant (A), from Eq. A7, the last three equations above may be combined to yield

$$I = \frac{k_R(I)k_E n_{cG}(\beta(I) - \beta_{Dark})}{A}, \quad \text{(B7)}$$

which relates I to $\beta(I)$ without the need for assumptions about the values of ν_{RE} and β_{sub}.

Any of the steady variables determined above, including $Ca(I)$, may readily be plotted as a function of intensity, e.g., $Ca(I)$ versus I, or as a function of any of the other steady variables.

APPENDIX C: A QUANTITATIVE MODEL OF RECOVERIN'S INTERACTIONS

Recoverin's Interactions with Calcium and with Rhodopsin Kinase

The calcium binding protein recoverin has been reported to be present in amphibian rods at a concentration of at least 30 μM (Kawamura, 1993), and more recently, as high as 140 μM (Kawamura et al., 1996). Bovine recoverin has two calcium binding sites, which bind calcium cooperatively with a Hill coefficient near 2, and an apparent $K_{1/2}$ of 4.5 μM in frog rods (Klenchin et al., 1995) and 17 μM in bovine rods (Ames et al., 1995). From these numbers alone, it is clear that recoverin will be important in buffering calcium in the rod.

In addition to its role as a calcium buffer, recoverin with two Ca^{2+} bound (Rec · 2 Ca) has been found to inhibit the phosphorylation of rhodopsin (Kawamura, 1993; Chen et al., 1995; Klenchin et al., 1995; Sato and Kawamura, 1997). This most likely occurs through the binding of Rec · 2 Ca to rhodopsin kinase (RK), which is thereby prevented from interacting appropriately with R*.

We believe that these two actions of recoverin, its calcium buffering and its inhibition of RK, are critical in describing certain calcium-dependent features of light-adaptation. Accordingly, we have developed a model of the binding interactions of recoverin, which is expressed in the chemical Scheme 1, which is similar to that in Erickson et al. (1998).

Analysis of the Model of Recoverin's Binding: Free Concentrations of Recoverin and RK

The experimental evidence supports the view that the binding of Rec to Ca^{2+} equilibrates very rapidly, as does the binding of myristoylated Rec · 2 Ca to disc membranes (Zozulya and Stryer, 1992; Ames et al., 1995). Accordingly, we treat all the interactions in Scheme 1 as effectively instantaneous, thus, enabling the use of equilibrium binding constants.

To analyze the system in Scheme 1, one first writes the equations defining the five equilibrium constants, K_1–K_5, and then the two conservation equations specifying the total quantities of recoverin and rhodopsin kinase, Rec_{tot} and RK_{tot}, respectively. In addition, from the thermodynamic principle that there can be no net movement around the reaction loop in Scheme 1, one obtains the interrelation that $K_5 = (K_2/M)(K_4/K_3)$. The concentrations of free recoverin and rhodopsin kinase, expressed in fractional form Rec/Rec_{tot} and RK/RK_{tot} are then found to be related by the equation

$$\frac{RK}{RK_{tot}} = 1/\left(1 + C_1\frac{Rec}{Rec_{tot}}\right), \quad \text{(C1)}$$

where the parameter C_1 is given by

$$C_1 = \left(\frac{Ca}{K_1}\right)^2\left[\frac{1}{K_3} + \frac{1}{K_4}\frac{M}{K_2}\right]Rec_{tot}. \quad \text{(C2)}$$

After some tedious algebra, one obtains the following quadratic equation for the fraction of free recoverin:

$$C_1C_2\left(\frac{Rec}{Rec_{tot}}\right)^2 + \left(C_1\left(\frac{RK_{tot}}{Rec_{tot}} - 1\right) + C_2\right)\frac{Rec}{Rec_{tot}} - 1 = 0, \quad \text{(C3)}$$

where the parameter C_2 is given by

$$C_2 = 1 + \left(\frac{Ca}{K_1}\right)^2\left(1 + \frac{M}{K_2}\right). \quad \text{(C4)}$$

Hence, one first evaluates the parameters C_1 and C_2, then solves the quadratic in Eq. C3 to obtain the fractional recoverin concentration, and finally substitutes this into Eq. C1 to obtain the fractional rhodopsin kinase concentration. The rate constant of R* inactivation is obtained by substitution in Eq. A12.

$$\begin{array}{ccccc}
\mathrm{Rec} + 2\mathrm{Ca} & \overset{K_1^2}{\rightleftharpoons} & \mathrm{Rec}\cdot 2\mathrm{Ca} + \mathrm{M} & \overset{K_2}{\rightleftharpoons} & (\mathrm{Rec}\cdot 2\mathrm{Ca})\cdot \mathrm{M} \\
 & & + \mathrm{RK_{aq}} & & + \mathrm{RK_{mem}} \\
 & & \Updownarrow K_3 & & \Updownarrow K_4 \\
 & & (\mathrm{Rec}\cdot 2\mathrm{Ca})\cdot \mathrm{RK_{aq}} + \mathrm{M} & \overset{K_5}{\rightleftharpoons} & ((\mathrm{Rec}\cdot 2\mathrm{Ca})\cdot \mathrm{M})\cdot \mathrm{RK_{mem}}
\end{array} \quad \text{(SCHEME 1)}$$

Recoverin's Calcium Buffering Power

Once the dependence of free recoverin concentration on free calcium concentration has been determined, the calcium buffering power contributed by recoverin can be calculated. Since recoverin has been assumed always to bind two Ca^{2+} ions, then its Ca^{2+}-buffering power (defined in terms of the total quantity of calcium, Ca_{tot}), can be expressed as

$$B_{Ca,\,Rec} = \frac{d\,Ca_{tot}}{d\,Ca} = -2\frac{d\,Rec}{d\,Ca}. \qquad (C5)$$

The right-hand side of Eq. C5 may be evaluated most simply by numerical differentiation of the relationship between *Rec* and *Ca*. Alternatively, it is possible to differentiate the quadratic expression in Eq. C3, taking care to note that C_1 and C_2 are not constants, but instead are functions of *Ca*. After some excruciating algebra, one obtains a very complicated analytical expression for $B_{Ca,\,Rec}$ that will not be presented here, but which agrees exactly with the numerical solution.

This work was supported by National Institutes of Health grant EY-02660 and a Jules and Doris Stein Research to Prevent Blindness Professorship (to E.N. Pugh Jr.), and by Wellcome Trust grant 034792 (to T.D. Lamb).

Submitted: 8 August 2000
Revised: 13 September 2000
Accepted: 15 September 2000

REFERENCES

Ames, J.B., T. Porumb, T. Tanaka, M. Ikura, and L. Stryer. 1995. Amino-terminal myristoylation induces cooperative calcium binding to recoverin. *J. Biol. Chem.* 270:4526–4533.

Baylor, D.A., and A.L. Hodgkin. 1974. Changes in time scale and sensitivity in turtle photoreceptors. *J. Physiol.* 242:729–758.

Baylor, D.A., T.D. Lamb, and K.-W. Yau. 1979. Responses of retinal rods to single photons. *J. Physiol.* 288:613–634.

Chen, C.-K., J. Inglese, R.J. Lefkowitz, and J.B. Hurley. 1995. Ca^{2+}-dependent interaction of recoverin with rhodopsin kinase as a regulatory mechanism in rhodopsin signaling. *J. Biol. Chem.* 270:1–7.

Cobbs, W.H., and E.N. Pugh Jr. 1987. Kinetics and components of the flash photocurrent of isolated retinal rods of the larval salamander *Ambystoma tigrinum*. *J. Physiol.* 394:529–572.

Cornwall, M.C., and G.L. Fain. 1994. Bleached pigment activates transduction in isolated rods of the salamander retina. *J. Physiol.* 480:261–279.

Dawis, S.M., R.M. Graeff, R.A. Heyman, T.F. Walseth, and N.D. Goldberg. 1988. Regulation of cyclic GMP metabolism in toad photoreceptors. *J. Biol. Chem.* 263:8771–8785.

Erickson, M.A., L. Lagnado, S. Zoyzula, T.A. Neubert, L. Stryer, and D.A. Baylor. 1998. The effect of recombinant recoverin on the photoresponse of truncated rod photoreceptors. *Proc. Natl. Acad. Sci. USA.* 95:6474–6479.

Fain, G.L., T.D. Lamb, H.R. Matthews, and R.L.W. Murphy. 1989. Cytoplasmic calcium as the messenger for light adaptation in salamander rods. *J. Physiol.* 416:215–243.

Fesenko, E.E., S.S. Kolesnikov, and A.L. Lyubarsky. 1985. Induction by cyclic GMP of cationic conductance in plasma membrane of retinal rod outer segment. *Nature.* 313:310–313.

Forti, S., A. Menini, G. Rispoli, and V. Torre. 1989. Kinetics of phototransduction in retinal rods of the newt *Triturus cristatus*. *J. Physiol.* 419:265–295.

Goldberg, N.D., A. Ames III, J.E. Gander, and T.F. Walseth. 1993. Magnitude of increase in retinal cGMP metabolic flux determined by ^{18}O incorporation into nucleotide alpha-phosphoryls corresponds with intensity of photic stimulation. *J. Biol. Chem.* 258:9213–9219.

Gray-Keller, M.P., and P.B. Detwiler. 1994. The calcium feedback signal in the phototransduction cascade of vertebrate rods. *Neuron.* 13:849–861.

Hodgkin, A.L., and B.J. Nunn. 1988. Control of light-sensitive current in salamander rods. *J. Physiol.* 403:439–471.

Jones, G.J. 1995. Light adaptation and the rising phase of the flash photocurrent of salamander retinal rods. *J. Physiol.* 487:441–451.

Kawamura, S. 1993. Rhodopsin phosphorylation as a mechanism of cyclic GMP phosphodiesterase regulation by S-modulin. *Nature.* 362:855–857.

Kawamura, S., and M. Murakami. 1986. In situ cGMP phosphodiesterase and photoreceptor potential in gecko retina. *J. Gen. Physiol.* 87:737–759.

Kawamura, S., O. Kuwata, M. Yamada, S. Matsuda, O. Hisatomi, and F. Tokunaga. 1996. Photoreceptor protein s26, a cone homologue of S-modulin in frog retina. *J. Biol. Chem.* 271:21359–21364.

Klenchin, V.A., P.D. Calvert, and M.D. Bownds. 1995. Inhibition of rhodopsin kinase by recoverin: further evidence for a negative feedback-system in phototransduction. *J. Biol. Chem.* 270:16147–16152.

Koutalos, Y., K. Nakatani, T. Tamura, and K.-W. Yau. 1995a. Characterization of guanylate cyclase activity in single retinal rod outer segments. *J. Gen. Physiol.* 106:863–890.

Koutalos, Y., K. Nakatani, and K.-W. Yau. 1995b. The cGMP phosphodiesterase and its contribution to sensitivity regulation in retinal rods. *J. Gen. Physiol.* 106:891–921.

Lagnado, L., and D.A. Baylor. 1994. Calcium controls light-triggered formation of catalytically active rhodopsin. *Nature.* 367: 273–277.

Lagnado, L., L. Cervetto, and P.A. McNaughton. 1992. Calcium homeostasis in the outer segments of retinal rods from the tiger salamander. *J. Physiol.* 455:111–142.

Lamb, T.D., and E.N. Pugh Jr. 1992. A quantitative account of the activation steps involved in phototransduction in amphibian photoreceptors. *J. Physiol.* 449:719–758.

Lyubarsky, A., S. Nikonov, and E.N. Pugh Jr. 1996. The kinetics of inactivation of the rod phototransduction cascade with constant Ca_i^{2+}. *J. Gen. Physiol.* 107:19–34.

Matthews, H.R. 1996. Static and dynamic actions of cytoplasmic Ca^{2+} in the adaptation of responses to saturating flashes in salamander rods. *J. Physiol.* 490:1–15.

Matthews, H.R. 1997. Actions of Ca^{2+} on an early stage in phototransduction revealed by the dynamic fall in Ca^{2+} concentration during the bright flash response. *J. Gen. Physiol.* 109:141–146.

Matthews, H.R., R.L.W. Murphy, G.L. Fain, and T.D. Lamb. 1988. Photoreceptor light adaptation is mediated by cytoplasmic calcium concentration. *Nature.* 334:67–69.

Murnick, J.G., and T.D. Lamb. 1996. Kinetics of desensitization induced by saturating flashes in toad and salamander rods. *J. Physiol.* 495:1–13.

Nikonov, S., N. Engheta, and E.N. Pugh Jr. 1998. Kinetics of recovery of the dark-adapted salamander rod photoresponse. *J. Gen. Physiol.* 111:7–37.

Pepperberg, D.R., M.C. Cornwall, M. Kahlert, K.P. Hofmann, J. Jin, G.J. Jones, and H. Ripps. 1992. Light-dependent delay in the falling phase of the retinal rod photoresponse. *Vis. Neurosci.* 8:9–18.

Pepperberg, D.R., D.G. Birch, K.P. Hofmann, and D.C. Hood. 1996. Recovery kinetics of human rod phototransduction inferred from the two-branched a-wave saturation function. *J. Opt. Soc. Am. A.* 13:586–600.

Pugh, E.N., Jr., S. Nikonov, and T.D. Lamb. 1999. Molecular mechanisms of vertebrate photoreceptor light adaptation. *Curr. Opin. Neurobiol.* 9:410–418.

Sato, N., and S. Kawamura. 1997. Molecular mechanism of S-modulin action: binding target and effect of ATP. *J. Biol. Chem.* 122: 1139–1145.

Smith, N.P., and T.D. Lamb. 1997. The a-wave of the human electroretinogram recorded with a minimally invasive technique. *Vision Res.* 37:2943–2952.

Torre, V., H.R. Matthews, and T.D. Lamb. 1986. Role of calcium in regulating the cyclic GMP cascade of phototransduction in retinal rods. *Proc. Natl. Acad. Sci. USA.* 83:7109–7113.

Torre, V., J.F. Ashmore, T.D. Lamb, and A. Menini. 1995. Transduction and adaptation in sensory receptor cells. *J. Neurosci.* 15: 7757–7768.

Zozulya, S., and L. Stryer. 1992. Calcium-myristoyl protein switch. *Proc. Natl. Acad. Sci. USA.* 89:11569–11573.